Ore Geology Reviews 81 (2017) 79–95

Contents lists available at ScienceDirect

Ore Geology Reviews

journal homepage: www.elsevier.com/locate/oregeorev

Tin-tantalum-niobium mineralization in the Penouta deposit (NW Spain): Textural features and mineral chemistry to unravel the genesis and evolution of cassiterite and columbite group minerals in a peraluminous system

Teresa Llorens González [a,b,*], Francisco García Polonio [a,b], Francisco Javier López Moro [a,b], Agustina Fernández Fernández [b], José Luis Sanz Contreras [c], María Candelas Moro Benito [b]

[a] Strategic Minerals Spain, S.L., P° Recoletos, 37, 28004 Madrid, Spain
[b] Dept. of Geology, University of Salamanca, Plaza de los Caídos s/n, 37008 Salamanca, Spain
[c] Dept. of Geological and Mining Engineering, Higher Technical School of Mines and Energy Engineering, Polytechnic University of Madrid, C/ Ríos Rosas, 21, 28003 Madrid, Spain

ARTICLE INFO

Article history:
Received 29 April 2016
Received in revised form 24 October 2016
Accepted 28 October 2016
Available online 01 November 2016

Keywords:
The Penouta rare-element granite
Sn-Ta-Nb granites
Columbite group minerals
Fractional crystallization
Fluorine influence

ABSTRACT

The Sn-Ta-Nb Penouta granite is a highly evolved rare-metal post-kinematic leucogranite located in northwestern Spain, which was intermittently mined from Roman times until 1985, when falling metal prices led to the closure of most mines in the country.

Mineralization consists mainly of cassiterite (cassiterite I) and columbite group minerals (CGM) disseminated in the leucogranite, that increase in abundance and crystal size towards the upper part of the granitic cupola, especially in banded pegmatite-like dikes. Upwards quartz veins and greisen zones associated with the wall rock (mainly augen gneisses) were developed, containing coarse-grained cassiterite (cassiterite II). In contrast to nearly homogenous cassiterite chemistry, CGM may show complex compositional zonation patterns in relation with compositional variations of the leucogranite. Taking into account the mineral chemistry and textural features of CGM, two main groups were distinguished: (i) the first one (Group I) follows a general main trend from columbite-Fe to columbite-Mn, and finally to tantalite-Mn, which is in accordance with the evolution of the magma observed from the less to the more evolved zones of the leucogranite and from bottom to top of the body, and responds to common fractionation patterns of decreasing Nb/Ta ratios in the melt; and (ii) a second group (Group II), with intermediate values of Mn/(Mn + Fe) and Ta/(Ta + Nb) due to local supersaturation effects of the melt during crystallization, resulting in complex oscillatory zoned CGM crystals.

Textural and chemical features of cassiterite and CGM support the magmatic origin for both minerals, although cassiterite crystallized later in the sequence in both generations. Mineral chemistry evolution of CGM is in good agreement with a greater solubility of tantalite in the melt at the upper levels, where, besides, the fluorine contents of apatite and muscovite were increased and the onset of fluorite crystallization occurred. So, the fluorine enrichment in the upper levels seems likely to be an important component to explain the mineral chemistry of the Penouta granite, although the same mineral chemistry scheme could also be explained in terms of white mica fractionation upwards. Furthermore, the absence of typical textures originated by fluids in the CGM as well as the lack of these minerals in the quartz veins point to a low influence of the hydrothermal fluids in dissolution and recrystallization processes of the primary oxides.

1. Introduction

Tin and tantalum mineralization is represented worldwide by several giant mines that have historically been the main source of these metals. Most of them correspond with large pegmatite bodies, although rare-element granites are also well represented. This is the case of Greenbushes and Wodgina, in Australia (Fetherston, 2004; Partington et al., 1995; Sweetapple, 2000), Yichun and Nanping in China (Huang et al., 2002; Rao et al., 2009) or Tanco, in Canada (Černý et al., 1996).

Central Africa is considered to be as one of the world's largest reservoirs of Ta-bearing minerals, although the mining of those ores under conflict conditions led to dealing among the International Community to audit supply chains by means of fingerprinting tantalum ores (Melcher et al., 2008, 2015, 2016). Thus, the development of other

* Corresponding author at: Strategic Minerals Spain, S.L., C/ Vertical V, 16, Pol. Ind. Montalvo III, 37188, Carbajosa de la Sagrada, Salamanca, Spain.
E-mail address: tllorens@strategicminerals.com (T. Llorens González).

http://dx.doi.org/10.1016/j.oregeorev.2016.10.034
0169-1368/

conflict-free deposits has become a primary task to respond to the increasing demand of this product, especially in the technological industry. Russia is currently the only country in Europe where tantalum is mined (Pekov, 2000), although several potential projects can be also considered, such as alkaline intrusives of the central part of the Kola Peninsula, in Russia, Li-Sn-Ta-bearing pegmatites in Finland and the Beauvoir granite in the French Central Massif (Boyd, 2012). This is also the case of the Penouta Sn-Ta-Nb granite, in Spain, which contains

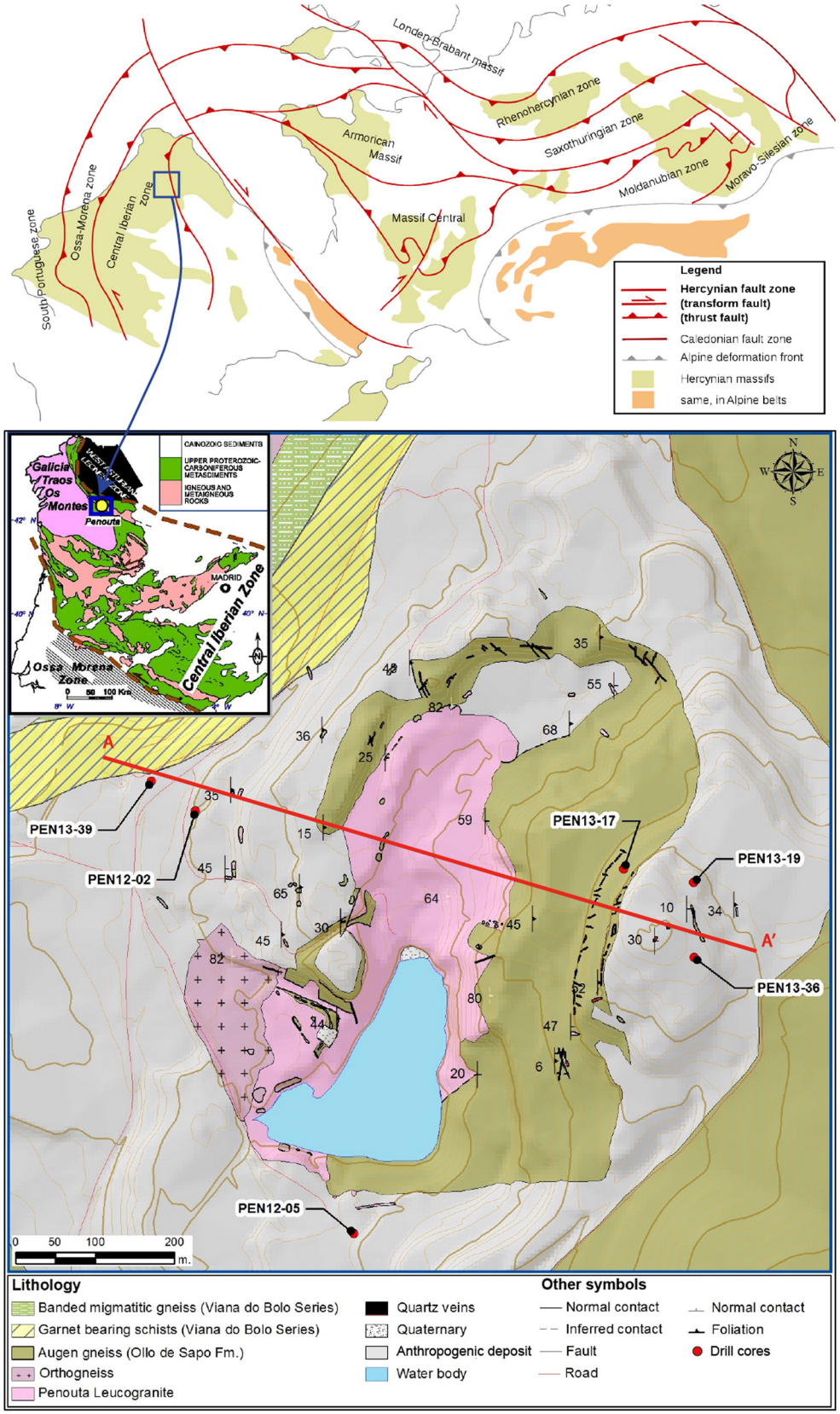

Fig. 1. Geological map of the Penouta ore deposit to the southwest extension of the Sn-W European Variscan Belt and location of the main drill holes studied.

95.5 Mt of Measured and Indicated Mineral Resources with average grades of 77 ppm Ta and 443 ppm Sn.

The north-western part of Spain, which belongs to the southwest extension of the Sn-W European Variscan Belt (Fig. 1), has been extensively explored and mined for tin and tantalum since the early twentieth century. The Penouta granite, located in the eastern part of the province of Ourense, is one of the best known Variscan Sn-Ta-Nb deposits from the Iberian Massif, together with the districts of Golpejas (Arribas et al., 1982), Trasquilón (García Guinea and Martínez Frías, 1992), Navasfrías (Llorens and Moro, 2010, 2012a,b) Argemela (Charoy and Noronha, 1996), Fuentes de Oñoro (Gonzalo and Gracia, 1985) and Ponte Segade (Canosa et al., 2012). These deposits have in common mineralization that occurs as disseminations throughout small granite bodies, with the highest grades of tin and tantalum in the apical zones.

Historically, mining in the Penouta area has been carried out since Roman times, with small underground tunnels which followed cassiterite mineralized quartz veins hosted by a peraluminous albite leucogranite. Mining in the Penouta deposit is documented since 1906, but it was not extensively exploited until the 1970s, mainly to obtain cassiterite from a granitic cupola and a swarm of related hydrothermal quartz veins, while Ta was obtained as by-product. Mining during this period was carried out by open pit methods, specifically targeting the kaolinized leucogranite and those portions of the country rock which had been muscovitized and were soft enough to be extracted using free dig methods. These materials were not milled and only fragments up to 2 mm in size were treated in the gravity plant, so that a great amount of cassiterite and columbite-group minerals (CGM) was not liberated from the hosting rock and was progressively accumulated in the tailings ponds. As a consequence, sands from tailings reached similar grades as those of the original granite.

From 1961 to 1985 several exploration projects were carried out in the Penouta granite, together with feasibility studies and drilling campaigns, including the study of not only cassiterite but also Ta-Nb-bearing minerals. These comprise mineral estimation projects and evaluation of mud pits, together with several drill hole campaigns to investigate resources and viability of the mining project, considering 13 Mt of reserves and average grades of 750 ppm Sn and 90 ppm Ta (ADARO, 1982, 1985). However, the drop of metal prices led to the definitive closure of the mine in 1985, after being acquired by different owners.

Thus, scarce scientific research has been carried out on the deposit, and most efforts were focused on developing adequate processing methods to separate metals from the old tailing dumps and the leucogranite matrix. However, the lack of detailed mineralogical information hindered separation of metals from sands. The revival of mining in recent years has encouraged the mining company Strategic Minerals Spain to carry out new exploration on the resources of the Penouta deposit. These jobs permitted the study of numerous drill holes throughout the entire deposit, so that a detailed characterization of the Sn- and Ta, Nb-oxide minerals could be completed.

In order to understand the genesis of the deposit and to determine the factors controlling the mineralization, textural and chemical evolution of the Sn and Ta-Nb-oxide minerals has been defined both vertically and horizontally in the granitic body. Several field and drilling campaigns have been carried out, together with an extensive sampling of the ore, which have provided detailed information about the mineralogy and chemistry of these minerals in the Penouta granite, which had not been studied before.

2. Material and methods

Mineralized samples were collected systematically from a variety of diamond drill holes with 250 m of average depth, which were carried out throughout the entire deposit of Penouta (Fig. 1) to define the type of mineralization present in the ore. A total of 111 samples were taken from 36 drill holes as well as 10 surface samples from the old open pit. Representative mineralized samples were selected from different drill holes to study thin sections. Additionally, two complete drill holes were sampled to analyze textural and chemical variations of the mineral phases from top to bottom and laterally in the deposit.

Detailed petrographic and textural studies were carried out by optical and electron microscopy at the University of Salamanca. Backscattered electron images and semi-quantitative analyses were obtained using the SEM (ZEISS DSM 940 equipped with EDX Z II by Tracor Northern system) to determine the compositional variations and zoning of the Sn, Nb and Ta minerals.

We also employed a Cameca SX-100 electron-microprobe at the Scientific-Technical Services of the University of Oviedo, which was operated with an accelerating voltage of 15 kV and a sample current of 15 nA. The counting time was 20 s for Fe, Ta, U and Al and 10 s for the rest of elements. The following standards were used: metals for Ti, Ta and Nb, zircon for Zr, cassiterite for Sn, magnetite for Fe, $MnTiO_3$ for Mn, wollastonite for Ca, albite for Na, orthoclase for K, apatite for F, corundum for Al, ThO_2 for Th and UO_2 for U. Data were reduced using the PAP routine (Pouchour and Pichoir, 1984, 1985). LiO_2 and B_2O_3 were determined by La-ICP-MS analysis with a laser ablation system UP213 Nd:YAG (NewWave) coupled to a Thermo Fisher Scientific iCAP Qc quadrupole ICP-MS instrument with enhanced sensitivity through a dual pumping system, at the Geochronology and Isotope Geochemistry-SGIker facility of the University of the Basque Country (Spain).

XRD patterns for clay materials were recorded using a Bruker D8 Advance Θ-2Θ diffractometer at the University of Salamanca, operating at 25 °C, 30 kV and 30 nA. The software DIFRACTplus were used for acquisition and treatment of diffraction data and the PDF-2 (2004) database were employed for mineral identification.

Binary and triangular distribution diagrams have been generated by the Geochemical Data Toolkit for Windows (GCDkit, Janoušek et al., 2006).

3. Geological setting

The Penouta Sn-Ta-Nb deposit is located in the Central Iberian Zone (CIZ), to the innermost part of the Iberian Variscan Belt, where two main formations crop out: the Viana do Bolo Series and the Ollo de Sapo Formation.

The Viana do Bolo Series (Early Cambrian) consists of high-grade metamorphic rocks, including banded migmatitic gneisses, garnet-bearing schists, marbles, calcium silicate rocks and scarce amphibolites, but only the two first crop out close to the Penouta granite (Fig. 1). The thickness of these rocks is estimated at a minimum of 1500 m. Furthermore, biotite-bearing orthogneiss appears intercalated in the Viana do Bolo Series close to the Penouta mine. Although it is undated, other equivalent orthogneisses (Covelo and San Sebastian orthogneisses) yielded ages of 487 ± 4 Ma and 470 ± 3 Ma respectively (Montero et al., 2009).

The Ollo de Sapo Fm. overlies the Viana do Bolo Series. It is a volcanogenic sequence of ca. 2000 m thick, which consists of augen gneisses, epiclastic tuffs and ignimbrites. Only the augen gneiss partially migmatized surfaces nearby the Penouta granite (Fig. 1). It is the most characteristic and abundant rock type, which shows porphyroclastic texture due to large K-feldspar and quartz porphyroclasts and intense deformation. The metamorphic grade reaches the sillimanite isograd, and the U-Pb zircon dating yielded ages of 472 ± 14 Ma (Díez Montes et al., 2010).

The structural scheme is the result of superposition of the three main Variscan deformational phases, which developed overturned to recumbent folds with E and NE vergence (D1), thrusting due to emplacement of a large nappe stack formed of allocthonous terranes (D2), and subvertical structures including upright folds and shear zones with mostly dextral wrench components (D3), the latter commonly related to Sn-W, Au and U mineralizations in the Iberian Massif (e.g.

González-Clavijo et al., 1993; López-Moro et al., 2013; Pereira et al., 1993). The late development of a gneiss dome due to a second extensional episode, together with normal faults such as that of Chandoiro, represents the late stages of gravitational collapse of the orogeny (Díez Montes, 2006). Late-Variscan fracture systems developed minor structures along N-S, NE-SW and E-W directions.

4. The Penouta deposit

The Penouta Sn-Ta-Nb leucogranite intruded the Viana do Bolo Series and the Ollo de Sapo Fm. after the main Variscan deformational phases, as suggested by the metamorphic textures of the host rocks cut by the intrusion. It is a sheet-like albitized and greisenized granitic cupola elongated in a SW-NE direction with a maximum length of about 1100 m and maximum width EW of 700 m (Figs. 1, 2, 3a). The body extends more than 200 m in depth, as only few drill holes more than 250 m deep cut the bottom of the granite. Petrographically, this fine- to medium-grained granite is leucocratic, hollocrystalline, white grey to greenish grey (Fig. 3b). It is mainly composed by quartz, muscovite, albite and K-feldspar, increasing contents of the two first towards the western zone of the deposit (muscovite-albite leucogranite), in contrast to eastern zones of the granitic cupola, where albite dominates in the mineralogical composition (albite leucogranite, Fig. 2). Zircon is a common accessory mineral, together with garnet and beryl, which increase considerably in some zones of the deposit and tourmaline occurs less frequently. Apatite and monazite are scarce in the granite, in agreement with the low bulk P contents reported by the geochemistry (<0.07 wt.%). Mineralization consists of cassiterite and CGM finely disseminated throughout the granite, increasing contents and size towards the apical zone, where intense kaolinization of the granite occurs. The Penouta granite is slightly to strongly peraluminous, with ASI values ranging from 1.05 to 1.83 [ASI being the $Al_2O_3/(CaO + Na_2O + K_2O)$ molar ratio]. Na_2O contents range from 2.5 to near 8, with the highest budget in the albite leucogranite samples from the top and eastern sections, where albite constitutes more than 60 % in weight of the granite.

Occasionally, banded pegmatitic-aplitic dikes (BPA) can be found in the Penouta granite, specifically occurring in the apical zone of the granitic cupola. These bodies show tabular shape, centimeter to meter thickness, and intruded the Penouta granite and the host metamorphic augen gneiss with low (nearly horizontal) to medium angles. The best expression of these bodies crops out to the eastern zone of the deposit, reaching 10 m in thickness. They are mainly composed by K-feldspar, albite, quartz and muscovite, as well as accessory beryl, apatite and garnet (Fig. 3c,d). The smallest BPA show a banded structure that consists of centimeter-wide layers composed by different proportions of the main constituents (e.g.: quartz-mica layers, albite layers and quartz layers) rhythmically interbedded. In contrast, the thickest bodies are better defined, showing fine-grained external zones of granitic composition, followed by intermediate zones mainly composed of blocky feldspar in a quartz-mica-bearing matrix alternating with fine-grained quartz-mica and albite layers as well as quartz layers. Cassiterite and CGM also occur disseminated in the BPA bodies, especially in the albite layers.

The cupola system culminates with the development of a stockwork of quartz veins up to 2 m thick (Fig. 3a), differentiating a group of subhorizontal veins slightly dipping to the E, and a second group of NE subvertical veins. They are sigmoidal, lenticular and tabular in shape and composed by colorless to milky quartz. Coarse-grained cassiterite crystallized related to the muscovite-rich selvages. Veins hosted by the Penouta leucogranite are uncommon, tabular in shape and not thicker than 30 cm.

Crystallization of these quartz veins occurred simultaneously with a strong greisenization of the hosting augen gneiss and the granitic cupola, giving rise to the development of an irregularly distributed greisen body throughout the eastern zone of the deposit. Greisen is mainly composed of fine- to coarse-grained quartz and mica, with accessory spessartine (here interpreted as part of the endogreisen), beryl, apatite and molybdenite (Fig. 3e), as well as cassiterite and accidental CGM. It is also common to find greisenized albite centimeter-thick veins intruding the host augen gneiss, which are mainly composed of coarse-grained muscovite disposed perpendicularly to the borders and a core of fine-grained albite containing cassiterite and CGM (Fig. 3f).

Finally, late centimeter-wide breccias were sealed by quartz/microcrystalline silica accompanying by clays, especially kaolinite. In some zones of the deposit this late structures show higher thickness, crosscut the granite and contain sulphides such as pyrite, galena and sphalerite, together with abundant barite and carbonates (Fig. 3g).

5. Results

5.1. Mineralogy and petrography of the Penouta leucogranite

The Penouta leucogranite is mainly formed by plagioclase, quartz, K-feldspar and white mica as essential minerals, varying gradually in different proportions, from muscovite-albite facies to the western and deeper zones, to albite leucogranite containing more than 50% albite

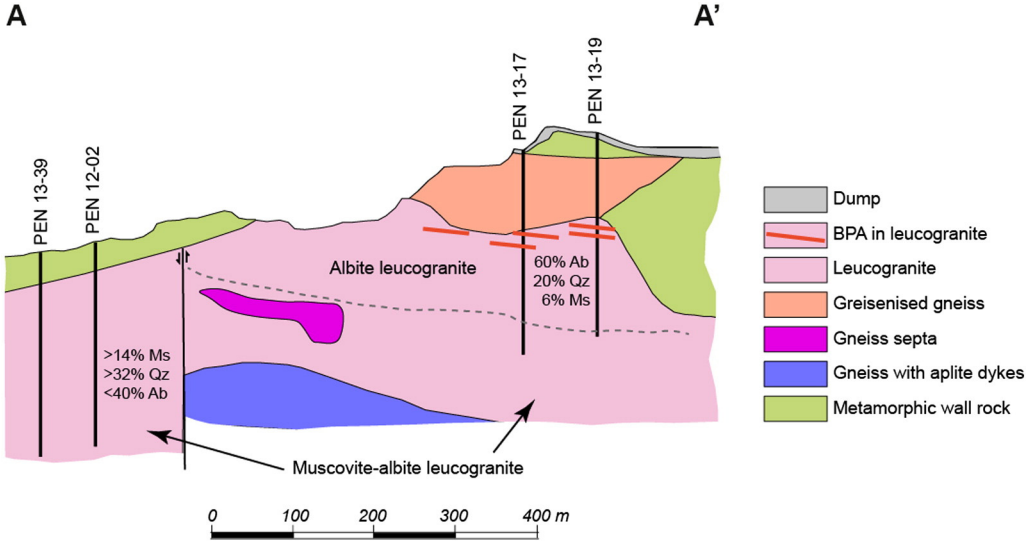

Fig. 2. Schematic cross section of the Penouta deposit (see location of the A-A′ section in Fig. 1) showing the main mineralogical changes of the leucogranite facies from west to east and from bottom to top, as well as the location of drill holes.

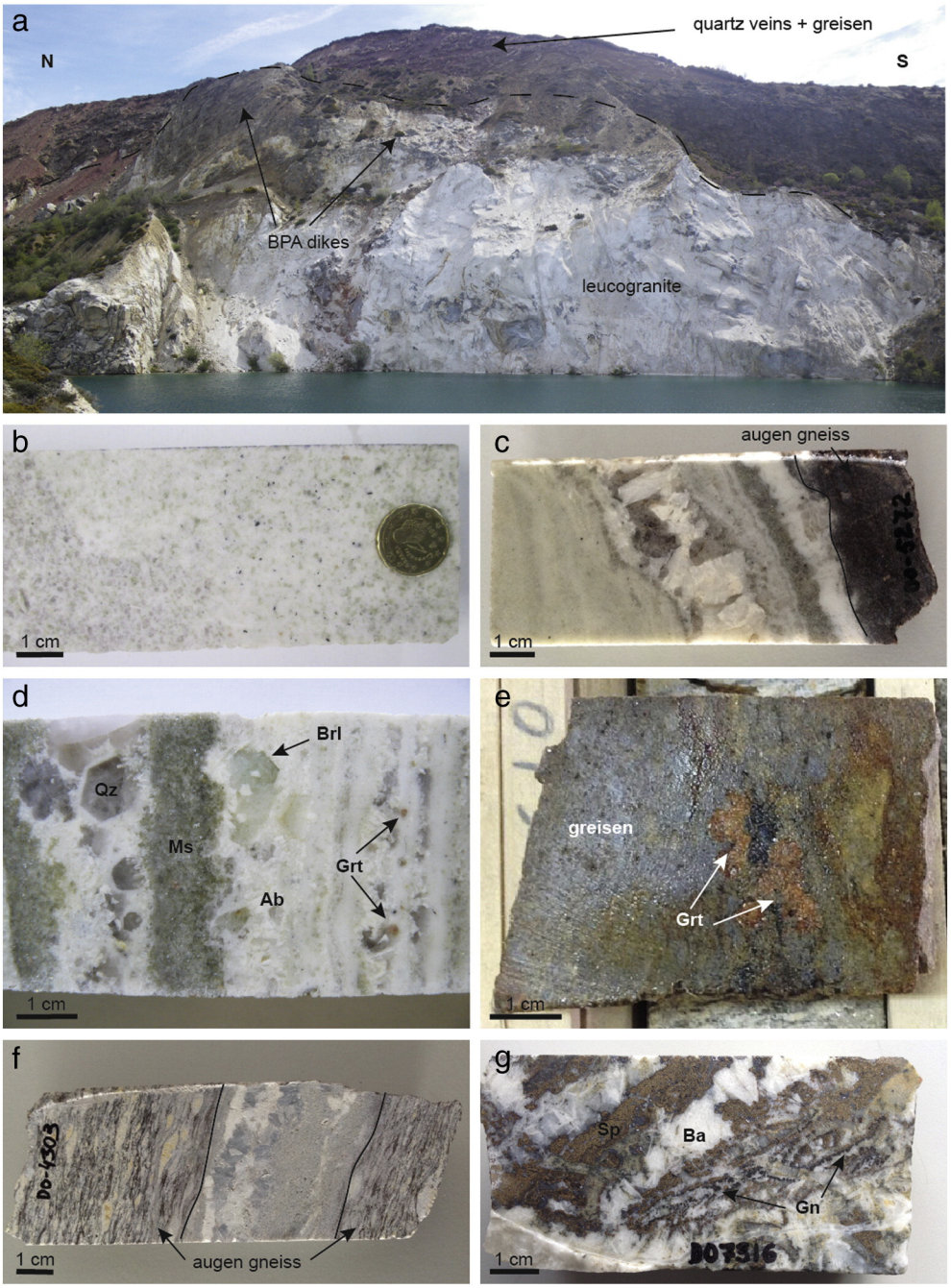

Fig. 3. a) General view of the old open pit of the Penouta leucogranite, showing a swarm of quartz veins and greisenized host metamorphic rock towards the cupola zone; b) typical sample of the Penouta albite leucogranite in a drill hole section, showing abundant disseminated cassiterite ± CGM mineralization (black spots); c) example of a banded pegmatitic-aplitic dike (BPA) hosted by the Ollo de Sapo augen gneiss, showing cassiterite ± columbite-tantalite mineralization (black spots); d) rhythmic alternation of albite and muscovite layers in a BPA dike, with crystallization of euhedral beryl and quartz; e) centimeter-sized crystals of Mn-bearing garnet in a greisen zone from the cupola; f) example of greisen vein containing fine-grained albite, hosted by the augen gneiss; e) mineralization of sphalerite + galena + barite ± carbonates filling late fractures and veins. Qz: quartz, Ms: muscovite; Brl: beryl; Ab: albite; Grt: garnet; Sp: sphalerite; Ba: barite; Gn: galena.

to the eastern and shallower areas of the deposit (Fig. 2). *Quartz* varies from common millimeter size crystals in deeper zones of the deposit to rounded crystals with snowball texture containing abundant albite inclusions in the upper zones. The albite leucogranite facies also show centimeter size patches of quartz in the granite matrix. Regarding *feldspars s.l.*, albite (Ab_{97-98}) is the most common, increasing in abundance towards the eastern zones of the deposit, reaching 68 wt.%. K-feldspar (Or_{92-98}) is less abundant and commonly replaced by albite. *White mica* commonly replaces feldspars and is usually associated with other late minerals such as beryl and cassiterite. Its chemical composition varies between muscovite and phengitic mica containing up to 5.27 wt.% FeO, showing a notorious Mg enrichment towards the BPA and greisen, where the lowest Ti contents are observed.

Among accessory minerals, *garnet* is relatively abundant throughout the Penouta deposit (Fig. 3d,e), disseminated or concentrated in albite-rich patches throughout the granite. It shows compositional variations from $Alm_{51}Sp_{44}$ in the deeper zones of the muscovite-albite leucogranite, to $Sp_{79}Alm_{13}$ in the upper zones of the albite leucogranite and greisen, thus reflecting an increase in Mn contents towards the cupola. It has been commonly altered to chlorite. *Zircon* occurs as cloudy crystals disseminated throughout the granite, containing up to 16 wt.% Hf in the upper levels, which is a common feature of extremely

differentiated granites, such as that of Yichun (Huang et al., 2002) and Považský Inovec Mountains (Chudík et al., 2008), and pegmatites, e.g. Bastar-Malkangiri belt, Central India (Pal et al., 2007).

Fluorapatite is scarce in the granite, increasing considerably in the greisen and also commonly in small pegmatite bodies, where an intense superimposed albitization and higher F contents are observed (up to 0.836 apfu F in pegmatites). It is a late mineral in the paragenesis, as it commonly shows poiquilitic textures and crystallizes in association with cassiterite and CGM (Figs. 4, 5a). Compositionally it is enriched in Mn (up to 0.24 apfu), and crystals usually show cores slightly enriched in fluorine (Table 1). Another rare accessory phosphate in the Penouta granite is *monazite-(Gd)*, which displays a LREE- and MREE-rich composition and low ThO_2 contents, whereas that identified in the greisen reaches 20 wt.% ThO_2 and a lower MREE budget.

Tourmaline is not very common in the Penouta granite. It occurs as euhedral to subeuhedral, millimeter to centimeter sized crystals, usually forming dendrite-like aggregates of an intense dark blue color (Fig. 5b), and seems to be a late mineral phase, as it has been identified close to fracture zones. It has been classified as schorl belonging to the alkaline group (Figs. 6a,b, Table 2) and the alkali-subgroup 1 (Fig. 7), considering that generally F < 0.5 apfu and assuming V-site commonly occupied by OH (Henry et al. 2011). The main schorl-elbaite substitution vector is shown in the triangular diagram Fe–2Li–Mg (Fig. 6b). LiO_2 contents varies from 0.84 to 1.09 wt.%, typical of Li-bearing granitoids and related pegmatites (Henry and Guidotti, 1985) (Fig. 6c).

Beryl is a ubiquitous mineral phase in the Penouta granite as late millimeter sized crystals, usually with poiquilitic texture. It is also common in the greisen zone in close association with cassiterite and sulphides (sphalerite and molybdenite), and in the BPA as euhedral centimeter sized crystals (Figs. 3d, 5c). Its chemical composition shows higher F contents upwards.

U-rich minerals are accessory minerals in the Penouta leucogranite and consist of *uraninite*, commonly coated by pyrite, and *autunite*, as green platy crystals and aggregates frequently coating fractures in the granite. Pink colored *fluorite* has been identified in few samples from the cupola (Fig. 5d).

The style of crystallization of *sulphides* varies depending on the hosting rock. Pyrite, arsenopyrite, sphalerite (black-colored, Fe-rich) and less frequently chalcopyrite, bismuthinite, native Bi and stannite sometimes occur disseminated throughout the deeper zones of the muscovite-albite leucogranite and close to fracture zones, as millimeter-size crystals or centimeter-size aggregates that are usually altered to the point of being replaced totally by Fe-oxide spots. Molybdenite has frequently been found in greisen-like sheets intruding the granite and BPA, as well as in the greisen body, forming euhedral millimeter-size crystals (Fig. 5c). Finally, late hydrothermal breccias founded in the northern and western parts of the Penouta deposit contain abundant massive or drusiform pyrite-marcasite coating the veins together with clays, and a typical association of galena, sphalerite (yellow-colored, Fe-poor) and prismatic centimeter-size crystals of barite (Fig. 3g).

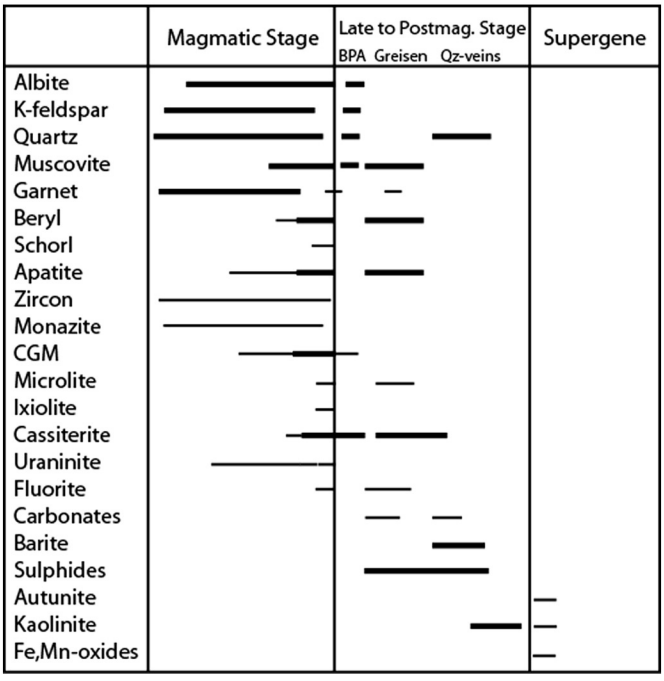

Fig. 4. Schematic paragenetic sequence of the minerals forming the Penouta deposit.

Clays are one of the most common supergene alteration products of the feldspars forming the Penouta granite and filling late fractures. XRD patterns permitted their identification as mainly kaolinite and smectite in a lesser extent. However, considering the well crystallized structure of kaolinite in some parts of the deposit, a late hydrothermal origin for this mineral is also suggested (Fig. 4).

5.2. Mineralogy and chemistry of Sn, Ta and Nb ore minerals

5.2.1. Cassiterite

A total of 81 analyses of cassiterite have been carried out, most of them corresponding with the two drill holes studied from top to bottom (Pen 13–17 and Pen 13–39, see Fig. 1) to determine possible evolutionary trends. Two generations of cassiterite have been defined attending to the deposit type and the mineral association.

Cassiterite I occurs disseminated in the Penouta leucogranite and the BPA as anhedral to euhedral crystals up to 2.2 mm in size, sometimes forming aggregates up to 1 cm length (Fig. 3b, 8a,b). Average size of crystals throughout the granite is around 100 μm, with maximum length in depth. This mineral usually exhibits a strong colored zoning that commonly responds to variations in the Mn, Fe, Nb and Ta contents, although without a distinctive pattern. It is mainly associated with albite to the eastern albite leucogranite and progressively with white mica and quartz to the western muscovite-albite granite, indicating a magmatic origin, although later than CGM, as suggested by zoned columbite crystals included (but not exsolved) in the cassiterite ones (Fig. 9a,b). Hole Pen 13–39 shows different association in deeper studied samples, as cassiterite crystals are mainly associated with beryl (Fig. 8b), suggesting that both mineral phases crystallized together.

Cassiterite II crystallized as millimeter to centimeter-sized, subhedral to euhedral crystals in greisenized zones of the cupola and quartz veins, both in the inner parts and towards the muscovite-rich borders, where typical twinning is observed and cassiterite commonly forms great aggregates of crystals (Fig. 8c). Cassiterite II is also related to those zones of the leucogranite where the hydrothermal alteration caused deposition of sulphides such as sphalerite and stannite (Fig. 8d).

Both generations of cassiterite are chemically very similar, showing a limited range of compositions, with considerable overlap in Ta, Nb, Fe and Mn values, whereas TiO_2 contents are negligible, reaching 0.2 wt.% (Table 3). Ta_2O_5 exceeds Nb_2O_5 in almost all analyzed crystals reaching commonly 4.0 wt.% and even 12.3 wt.% in the eastern apical zone of the albite leucogranite (the most evolved cupola zone), although average contents are around 2.0 wt.%. Only cassiterite from the western muscovite-albite leucogranite show more Nb_2O_5 than Ta_2O_5 contents. Most crystals show significant but low FeO contents, reaching 1.23 wt.% in some grains. These features are also observed plotting cassiterite analyses in the columbite quadrilateral (Fig. 10a), which indicates limited variations of Fe-Mn contents, but high variability of Ta-Nb.

Similarly, good 1:2 correlation between Fe + Mn and Nb + Ta (Fig. 10b) has been observed, corresponding to the ideal coupled substitution $3Sn^{4+} \leftrightarrow (Fe,Mn)^{2+} + 2(Nb,Ta)^{5+}$ in the cassiterite structure. This substitution vector is also observed in the (Sn + Ti)–(Nb + Ta)–(Fe + Mn) triangular diagram (Fig. 10c). Moreover, low Ti contents

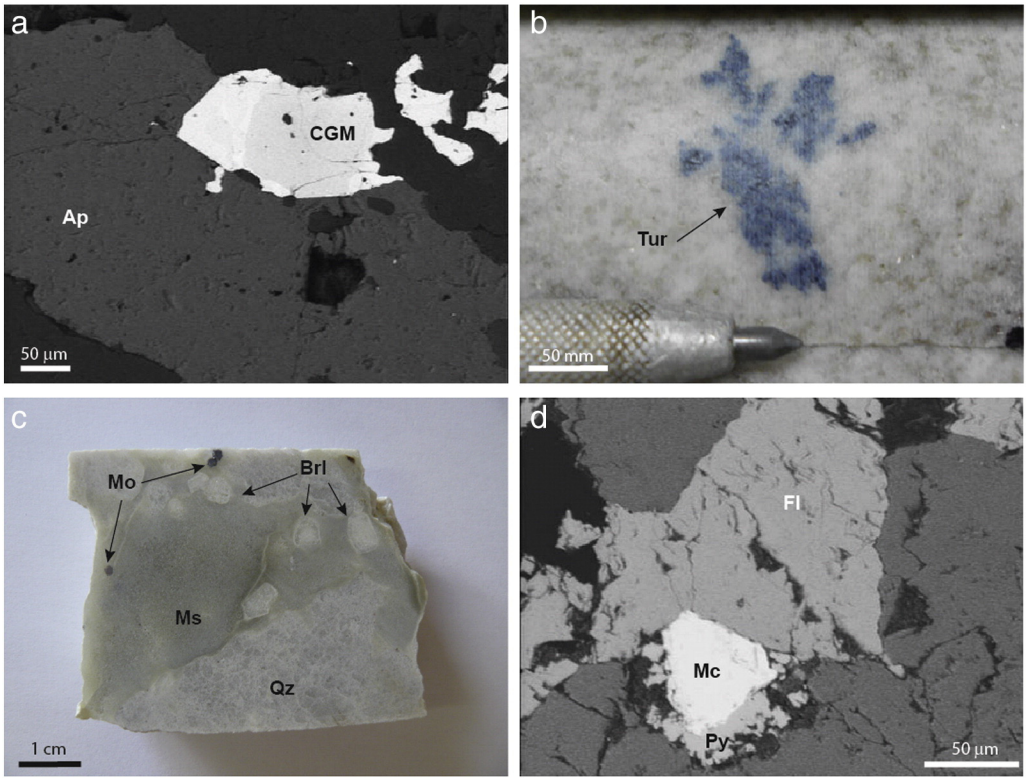

Fig. 5. a) Late fluorapatite crystal partially coating a zoned CGM; b) aspect of blue tourmaline aggregates in the leucogranite; c) Partially corroded beryl crystals in a fine-grained, strongly greisenized zone of the cupola, where millimeter-size molybdenite spots occurs; d) Fluorite from the greisenized cupola in association with an euhedral microlite crystal coated by pyrite. Ap: fluorapatite, CGM: columbite group minerals, Tur: tourmaline, Mo: molybdenite, Ms: muscovite, Qz: quartz, Brl: beryl, Mc: microlite, Py: pyrite, Fl: fluorite.

in all cassiterite crystals can be explained by direct substitution $Ti^{4+} \leftrightarrow Sn^{4+}$.

In order to constrain potential chemical differences of cassiterite in depth and laterally throughout the different facies of the Penouta leucogranite, Mn# [Mn/(Mn + Fe)] and Ta# [Ta / (Ta + Nb)] values were plotted *versus* depth for the two holes extensively studied (Fig. 11) and spaced about 1 km. These are Pen 13–39, sited to the western zone of the deposit, where muscovite-albite leucogranite crystallized, and Pen 13–17 to the eastern zone of the granitic cupola, dominated by albite-rich facies (see Fig. 2). Concerning the Ta# ratio, the western drill hole (Pen 13–39) exhibits high variability at intermediate depth, showing a slight decrease of average data and a sharp increase to the top. In contrast, limited variations are registered in hole Pen 13–17, with similar Ta# from the bottom to the inner parts and a sharp increase to the top, where BPA occur. However, a general Ta# increase upwards can be observed from bottom of Pen 13–39 to top of Pen 13–17, so that Ta enrichment is demonstrated both vertically and laterally in the deposit from the muscovite-albite leucogranite to the albite-rich one. Moreover, Mn# variations are less meaningful as a consequence of their limited variation range, remaining almost invariable in both facies of the leucogranite.

Table 1
Representative compositions of apatite from the Penouta leucogranite facies and BPA (wt.%) with their structural formulae (apfu).

	Muscovite-albite leucogranite		Albite leucogranite		BPA	
P_2O_5 (wt.%)	42.88	43.28	42.78	42.75	43.04	42.78
FeO	0.10	0.00	0.04	0.05	0.07	0.05
MnO	3.16	0.62	1.43	1.09	0.91	0.79
CaO	51.98	54.46	53.83	54.64	53.75	53.90
F	2.30	2.51	1.85	1.79	3.02	3.13
Cl	0.00	0.00	0.00	0.00	0.00	0.00
Total	100.43	100.86	99.92	100.31	100.80	100.66
Structural formulae calculated on the basis of 13 anions						
P (apfu)	3.242	3.251	3.213	3.197	3.273	3.268
Fe^{2+}	0.007	0.000	0.003	0.004	0.006	0.004
Mn	0.239	0.046	0.107	0.081	0.069	0.060
Ca	4.974	5.177	5.117	5.172	5.172	5.211
F	0.650	0.703	0.520	0.500	0.857	0.893
Cl	0.000	0.000	0.000	0.000	0.000	0.000
(OH)[a]	0.350	0.297	0.480	0.500	0.143	0.107

[a] OH contents are calculated by charge balance.

5.2.2. Ta-Nb-oxides

Ta- and Nb-oxides are ubiquitous minerals in the granitic rocks of the Penouta mine, crystallizing from the top to the bottom of the granitic body. However, they are not common in the greisen, and they never occur in the metamorphic country rocks or hydrothermal quartz veins. They show dark reddish, more commonly black color, and form prismatic (the reddish) or acicular crystals (the darker), the latter especially towards the apical zones of the albite leucogranite and BPA.

These minerals vary in composition and size more than cassiterite, both laterally and vertically in the Penouta deposit, although average size of crystals is normally constant, ranging between 40 and 80 μm, but with a range between 60 and 100 μm on average where the highest Ta contents occur (the upper levels of the eastern albite leucogranite). More variations were observed regarding maximum size of crystals. In the eastern zones maximum size of CGM increases from deeper (around 200 μm) to upper parts of the deposit (up to 580 μm in the BPA), whereas in the western muscovite-albite leucogranite the biggest CGM found in the upper part reach 340 μm, decreasing up to 100–140 μm in depth.

CGM are mainly in association with feldspars *s.l.*, especially in the eastern zone of the deposit, where the leucogranite shows the highest albite contents. Quartz and white mica are also commonly associated with the CGM (especially in the muscovite-albite leucogranite), less frequently cassiterite and only in some cases beryl and blue schorl. The

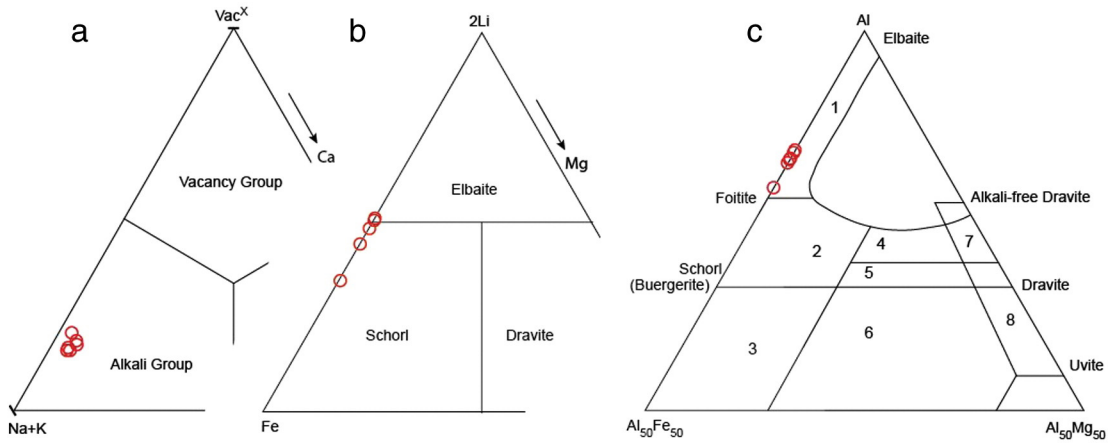

Fig. 6. Classification of tourmaline a) in the alkali group field of the Na + K–Vac^X–Ca triangular diagram; b) in the schorl field of the Fe–2Li–Mg triangular diagram (Henry et al., 2011); c) Plot of the tourmaline data in the field of Li-bearing granitoids and related pegmatites, modified after Henry and Guidotti (1985).

association with cassiterite can be so close that up to the 34% of CGM crystals may be included in cassiterite (deep samples of the muscovite-albite leucogranite).

Table 2
Representative compositions of schorl (wt.%) with their structural formulae (apfu) from the Penouta albite leucogranite.

	1	2	3	4	5	6
B_2O_3	10.52	10.36	10.44	10.17	10.39	10.73
SiO_2	36.38	36.53	36.24	36.58	36.13	36.21
TiO_2	0.02	0.00	0.00	0.03	0.00	0.00
Al_2O_3	34.13	34.02	33.34	33.94	34.24	33.78
FeO_t	8.97	9.15	12.21	9.65	9.74	10.03
MnO	1.36	1.35	0.97	1.35	1.46	1.47
MgO	0.01	0.01	0.01	0.01	0.01	0.00
LiO_2	1.02	1.01	1.09	0.92	0.95	0.84
CaO	0.27	0.23	0.32	0.23	0.28	0.16
Na_2O	2.38	2.41	2.33	2.43	2.30	2.30
K_2O	0.06	0.03	0.04	0.04	0.05	0.05
F	0.46	0.56	0.46	0.50	0.38	0.39
Cl	0.00	0.00	0.00	0.00	0.00	0.01
H_2O[a]	3.11	3.02	3.13	3.09	3.19	3.16
Total	98.70	98.68	100.59	95.86	95.93	96.07
Cations per formula unit normalized on the basis of 24.5 oxygen atoms						
B	3.096	3.049	3.057	2.982	3.048	3.159
T-site						
Si	6.202	6.227	6.150	6.212	6.141	6.176
Al	0.000	0.000	0.000	0.000	0.000	0.000
Z-site						
Al	6.000	6.000	6.000	6.000	6.000	6.000
Y-site						
Al Y	0.858	0.835	0.667	0.792	0.859	0.791
Fe^{2+}	1.279	1.305	1.733	1.371	1.384	1.431
Ti	0.002	0.000	0.000	0.004	0.000	0.000
Mg	0.003	0.003	0.004	0.003	0.002	0.001
Mn	0.197	0.195	0.139	0.195	0.210	0.212
Li	0.697	0.694	0.745	0.626	0.652	0.574
Total Y	3.036	3.031	3.288	2.991	3.107	3.009
X-site						
Ca	0.049	0.041	0.057	0.042	0.051	0.030
Na	0.787	0.796	0.767	0.799	0.757	0.760
K	0.013	0.006	0.010	0.010	0.011	0.011
^{X}Vac	0.151	0.157	0.166	0.150	0.182	0.198
Total X	1.000	1.000	1.000	1.000	1.000	1.000
V + W-site						
F	0.461	0.561	0.459	0.502	0.379	0.389
Cl	0.000	0.000	0.000	0.000	0.000	0.013
OH	3.539	3.439	3.541	3.498	3.621	3.598

B_2O_3 and LiO_2 were determined by LA-ICP-MS.
[a] H_2O was calculated by stoichiometry assuming OH = 4 − (F + Cl) apfu. The structural formulae have been calculated on the basis of 24.5 atoms of O following the general formula $XY_3Z_6T_6O_{18}(BO_3)_3V_3W$ (Hawthorne and Henry, 1999; Henry et al., 2011).

A total of 151 analyses of Nb-Ta oxide minerals have been carried out, most of them corresponding with CGM (Table 4). Samples are plotted in the four quadrants of the columbite diagram (Fig. 12a), although columbite-Mn is the better represented, followed by columbite-Fe and tantalite-Mn. Microlite and ixiolite are rare minerals in the Penouta granite and a secondary origin from previous CGM seems likely (Fig. 5d).

Two groups of CGM can be distinguished according to textural and chemical features (Fig. 12a). Group I follows a general main trend from columbite-Fe to columbite-Mn, and finally to tantalite-Mn, Ta# ranging between 0.06 and 0.76 and Mn# between 0.32 and 0.93 (dark grey line in Fig. 12a). These compositions correspond with more or less complex zoned CGM, showing Nb-rich cores commonly coated by Ta-rich rims, and reflect the evolution from the western zones of the muscovite-albite leucogranite towards the eastern albite leucogranite, as well as the Ta/Nb increase towards the upper part of the deposit (BPA, greisen), corresponding with the highest mineralization sectors. The presence of CGM in the greisen is interpreted as a consequence of alteration of the granite as greisenization occurred on top of the Penouta deposit, so that these crystals are relicts of previous CGM that have been

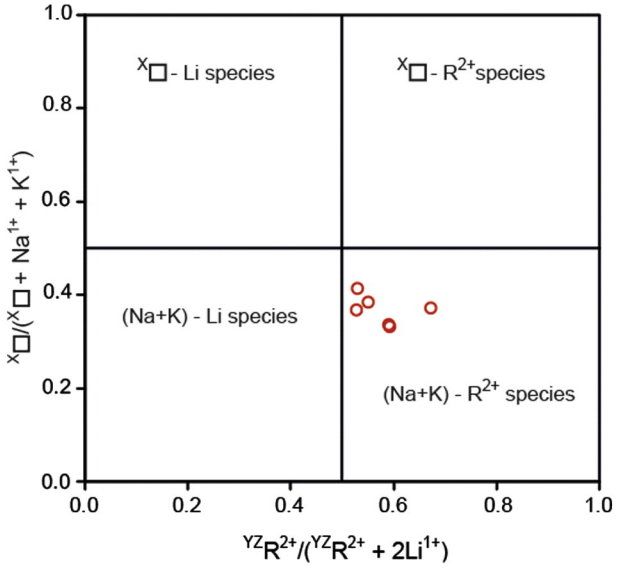

Fig. 7. Classification of tourmaline in the alkali-subgroup 1 (OH + F dominant), considering that generally $F^{1-} < 0.5$ apfu (see Table 2) and assuming V-site is commonly dominated by OH^{1-}. $^{YZ}R^{2+}$ represents the total number of divalent cations in the Y and Z sites (Henry et al., 2011).

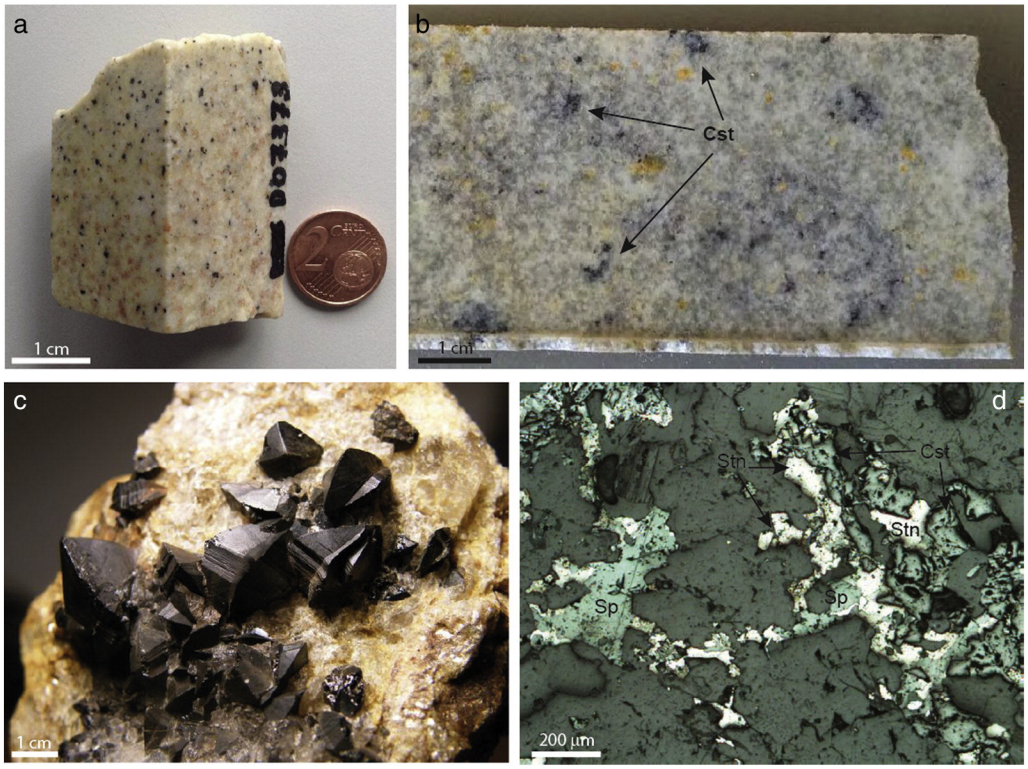

Fig. 8. Cassiterite types: a) Garnet-rich aplitic zone of the Penouta leucogranite showing abundant mineralization of disseminated cassiterite I ± CGM (black spots); b) cassiterite I aggregates associated with beryl in the Penouta leucogranite; c) typical euhedral cassiterite II crystals in a quartz vein from the greisenized cupola; d) fine-grained aggregates of cassiterite II in association with sulphides in a hydrothermally altered zone of the leucogranite. Cst: cassiterite, Sp: sphalerite, Stn; stannite.

partially corroded and altered. Group II evolves vertically in the diagram from columbite-Fe and columbite-Mn to Ta enriched compositions, Ta# ranging between 0.19 and 0.66 and Mn# between 0.30 and 0.74 (light grey line in Fig. 12a). Alteration and recrystallization patches belong to this group as well as complex internal zoning of some crystals found in almost all facies of the deposit.

Chemically, these minerals are characterized by low concentrations of minor elements, as observed in Table 4. Titanium contents are restricted, as only few crystals of columbite-Mn and columbite-Fe from the albite leucogranite and BPA contain up to 1.55 wt.% TiO_2, most of them belonging to the Group II of CGM. A sharp increase in TiO_2 contents can be distinguished in Fig. 12b as Ta# and Mn# decreases. Distribution of SnO_2 contents in the CGM, up to 1.4 wt.%, is very heterogeneous and in most cases controlled by association with cassiterite. Although scattering is high in Fig. 12c, a general trend to increase SnO_2 with increasing Ta# and Mn# ratios can be inferred. These low amounts of Sn and Ti plotted in the (Sn + Ti)–(Nb + Ta)–(Fe + Mn) triangular diagram of Fig. 12d denote variation along the border (Nb,Ta)–(Fe,Mn). Only the composition of the ixiolite crystal found in the BPA of the upper part of the deposit seems to follow the ideal trend defined by the substitution vector $(Fe,Mn)^{2+} + 2(Nb,Ta)^{5+} \leftrightarrow 3(Ti,Sn)^{4+}$ (Černý and Ercit, 1985; Černý et al., 1985b). Moreover, elevated concentrations of U (up to 0.77 wt.% UO_2) have only been recorded in few crystals of the columbite-Mn and tantalite-Mn from the albite leucogranite.

Detailed chemical variations of these minerals can be analyzed both laterally and vertically by plotting Ta# and Mn# ratios of cores and rims *versus* depth for holes Pen 13–39 and Pen 13–17 (Fig. 13). Thus, a slight reverse trend of decreasing average Ta# values can be drawn from bottom to top of the muscovite-albite granite, although crystal rims commonly display higher Ta contents than the cores. This reverse trend is followed by a sharp increase of Ta# to the top of the albite leucogranite, so that CGM deposited in BPA of the cupola display the highest Ta contents. Regarding the Mn#, high variability is observed in both facies, although a slight increase in crystal cores can be drawn from bottom to top. In this case, a Mn enrichment of the crystal cores relative to the rims in most samples is noticeable, especially for the albite leucogranite (Fig. 13).

5.3. Zoning patterns

Irregular zoning pattern were observed in several cassiterite grains regarding Ta, Nb, Fe and Mn and occasionally in Ta# and Mn#, showing Ta and Mn enrichment toward the rims of cassiterite, thus indicating an increase in Mn/Fe and Ta/Nb ratios in the melt with evolution.

Based on chemical and textural features, a wide variety of zoning patterns have been identified in the CGM due to Nb-Ta and Fe-Mn substitutions, although some unzoned crystals also occur:

Normal zoning: it is relatively common in the Penouta leucogranite, where many CGM show rather homogeneous Nb-rich cores, increasing progressively Ta contents towards the rims (Fig. 9c,d), according to a normal fractionation pattern of decreasing Nb/Ta ratios from core to rim of crystals (Černý and Ercit, 1985).

Oscillatory zoning: most crystals of CGM display oscillatory zoning characterized by episodic Nb- and Ta-rich zones alternating to each other, commonly forming thin and well defined layers from core to rim, parallel to the crystal edges (Fig. 9a,b,e,f). In other cases, alternating zones appear as sinuous bands or are truncated by later zones or patchy replacements (Fig. 9e). Sometimes this oscillatory zoning is progressive, evolving from Nb-rich cores to Ta-rich rims (Fig. 9a,f).

Reverse zoning: only few crystals show total or partial reverse zoning. In these cases the rim of the CGM crystals are Nb-enriched relative to the inner zones of the crystal (Fig. 14a,b), although it commonly responds to a later replacement event that truncates previous oscillatory or normal zoning.

Complex zoning: this zoning pattern is the most widespread in the Penouta granite. It consists of irregular patches of Nb- or Ta-rich phases superimposed to early columbite-rich phases, late infilling of

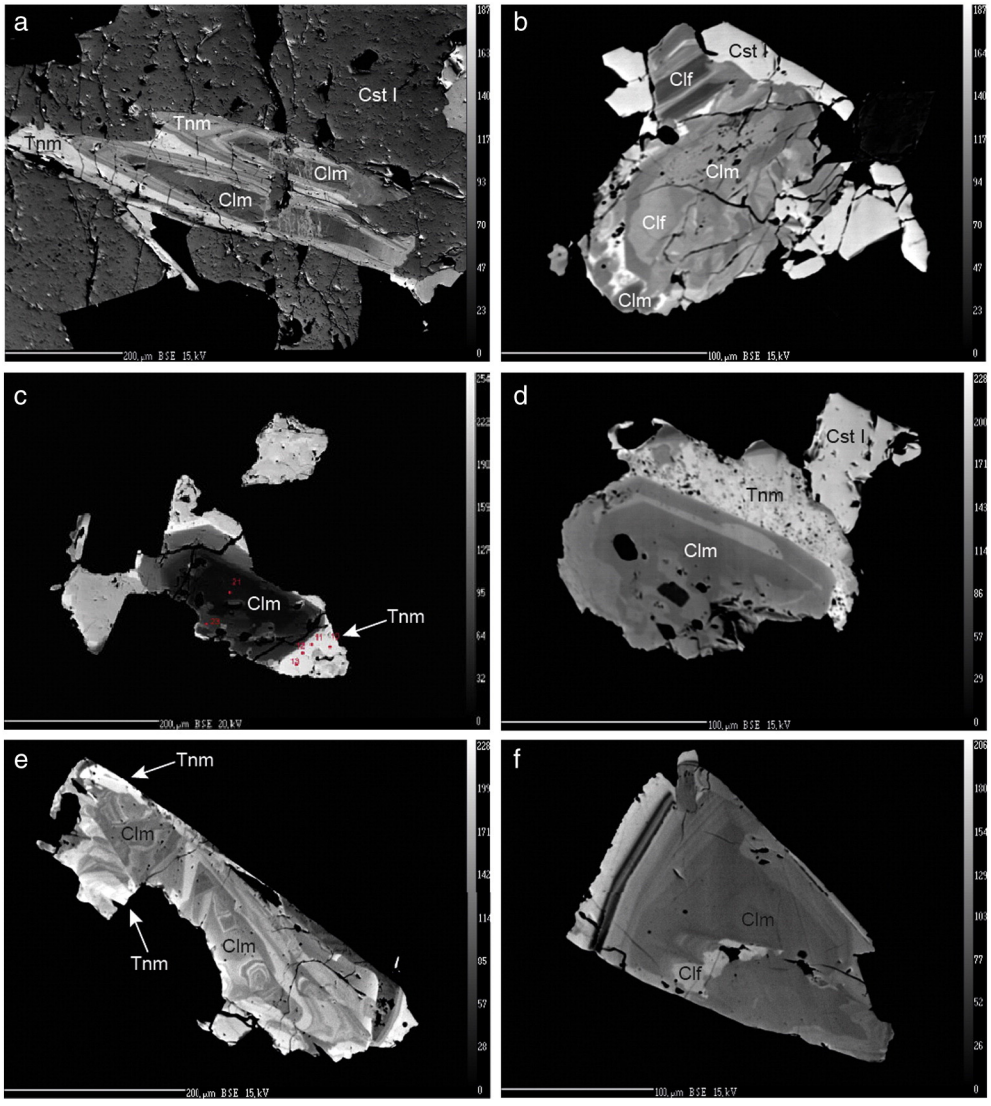

Fig. 9. BSE images of cassiterite and CGM: a) cassiterite I crystal including CGM with marked progressive oscillatory zoning; b) CGM with oscillatory to patchy zoning, reverse in some points, surrounded by late cassiterite I; c) normal zoned CGM from the open pit. Points 10, 11, 12 and 13 correspond with tantalite-Mn and points 21 and 23 with columbite-Mn; d) normal zoned CGM showing partial corrosion and reverse zoning towards some border zones; e) CGM from BPA with truncated oscillatory zoning, convoluted in some zones, and finally normal Ta enrichment; f) Oscillatory normal zoning, with late replacement by columbite-Fe. Cst: cassiterite, Clf: columbite-Fe, Clm: columbite-Mn, Tnm: tantalite-Mn.

Table 3
Representative compositions of cassiterite from the Penouta leucogranite facies, BPA and greisen (wt.%) with their structural formulae (apfu).

	Muscovite-albite leucogranite			Albite leucogranite						Garnet-rich aplite		BPA	Greisen
Nb_2O_5 (wt.%)	1.13	2.08	0.99	0.81	1.77	0.13	0.16	0.77	0.00	0.95	1.31	0.16	0.00
Ta_2O_5	3.87	1.25	2.16	12.35	3.43	1.80	1.50	2.26	1.41	0.46	3.44	1.70	3.71
TiO_2	0.03	0.00	0.00	0.01	0.01	0.00	0.02	0.01	0.00	0.02	0.00	0.12	0.00
SnO_2	93.79	95.22	96.06	84.43	93.46	98.01	98.72	96.79	98.80	98.49	94.60	98.49	96.03
FeO	0.67	0.89	0.70	1.26	1.01	0.28	0.15	0.69	0.07	0.26	0.73	0.28	0.05
MnO	0.17	0.11	0.09	0.72	0.11	0.00	0.04	0.08	0.00	0.01	0.03	0.02	0.00
Total	99.65	99.54	100.00	99.59	99.79	100.23	100.58	100.60	100.28	100.18	100.10	100.76	99.80
Structural formulae calculated on the basis of O = 2													
Nb (apfu)	0.013	0.023	0.011	0.009	0.020	0.001	0.002	0.009	0.000	0.011	0.015	0.002	0.000
Ta	0.026	0.009	0.015	0.086	0.023	0.012	0.010	0.015	0.010	0.003	0.023	0.012	0.026
Ti	0.001	0.000	0.000	0.000	0.000	0.000	0.000	0.000	0.000	0.000	0.000	0.002	0.000
Sn	0.941	0.950	0.959	0.860	0.934	0.980	0.983	0.962	0.987	0.980	0.944	0.978	0.968
Fe	0.014	0.019	0.015	0.027	0.021	0.006	0.003	0.014	0.001	0.005	0.015	0.006	0.001
Mn	0.004	0.002	0.002	0.016	0.002	0.000	0.001	0.002	0.000	0.000	0.001	0.000	0.000
Mn/(Mn + Fe)	0.202	0.108	0.114	0.367	0.104	0.000	0.214	0.104	0.000	0.024	0.037	0.066	0.000
Ta/(Ta + Nb)	0.673	0.266	0.569	0.901	0.539	0.893	0.853	0.637	1.000	0.226	0.612	0.868	1.000

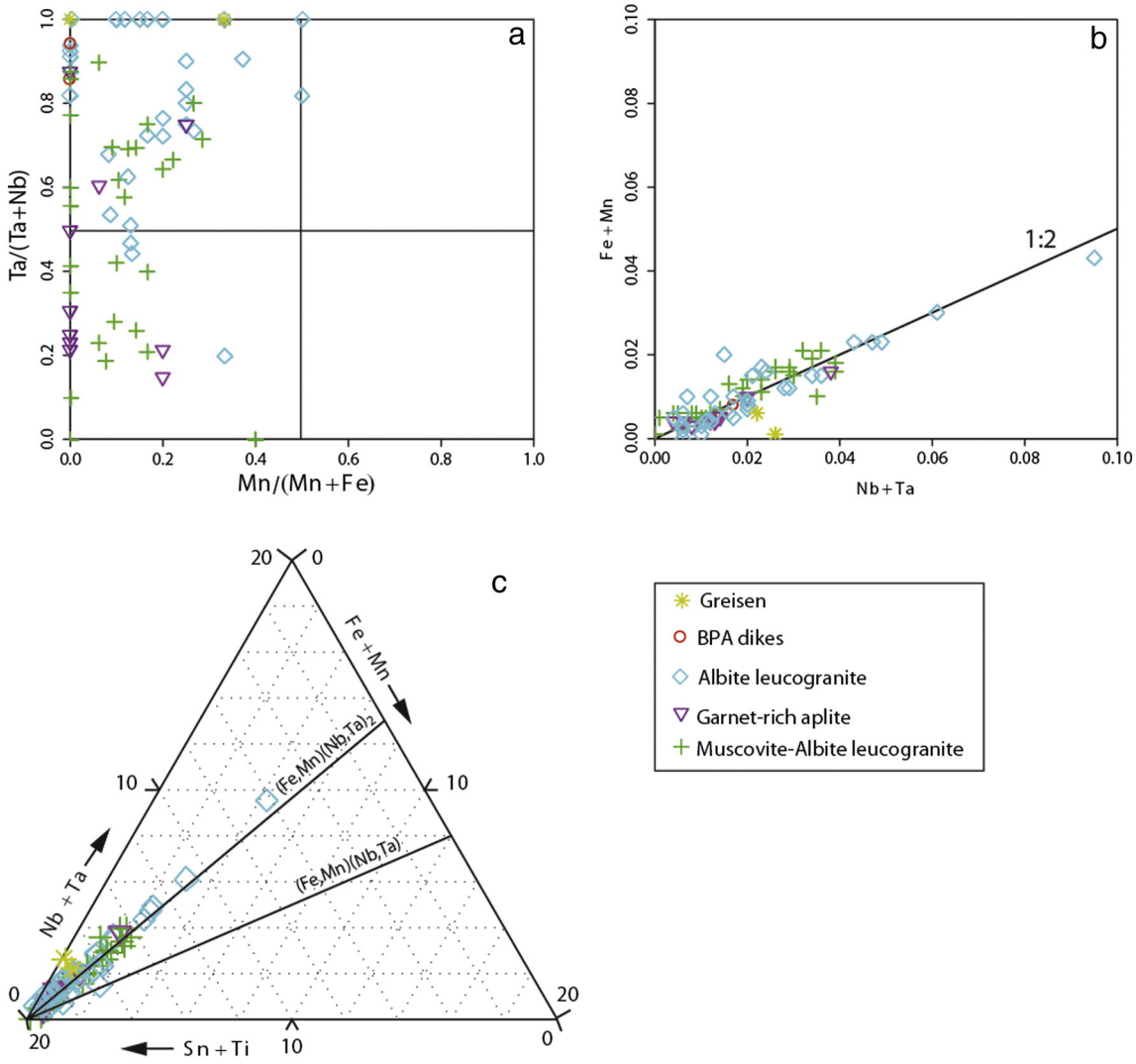

Fig. 10. a) Cassiterite analyses plotted in the columbite quadrilateral showing high Nb/Ta fractionation from muscovite-albite leucogranite to albite leucogranite; b) Good 1:2 correlation of the cassiterite analysis in the Nb + Ta *vs.* Fe + Mn diagram; c) Sn + Ti–Nb + Ta–Fe + Mn triangular diagram for cassiterite data, plotted along the $(Fe,Mn)^{2+} + 2(Nb,Ta)^{5+} \leftrightarrow 3(Ti,Sn)^{4+}$ substitution vector.

microveinlets and local inclusions of other Nb-Ta-oxides such as microlite, containing up to 1.34 wt.% UO_2, and ixiolite. Irregular convoluted zoning of border zones is also observed (Figs. 9b,e, 14b,c,d).

6. Discussion

6.1. Genesis of the Sn, Ta and Nb mineralization

The textural and chemical features of cassiterite and CGM can be used to determine the origin of the mineralization of the Penouta leucogranite. Mineral association and the disseminated mineralization style are major indicators of the magmatic origin of both minerals, although cassiterite crystallized later than CGM, as supported by the former overgrowing zoned columbite crystals (Fig. 9a).

Regarding CGM, differences in the associations are related to mineralogical variations in the different zones of the deposit. Thus, these minerals are commonly associated with albite in the eastern zones, decreasing to the western part of the deposit where feldspars decrease as quartz and white mica increase. This fact suggests that CGM crystallized during the magmatic stage instead of hydrothermal stage, as they are not related with late hydrothermal minerals such as barite, sulfides, apatite, or hydrothermal quartz and white mica. This is in consonance with recent investigations on fluid and melt inclusions and experimental research carried out in similar rocks (e.g. Badanina et al., 2004; Linnen, 1998), supporting the notion that CGM are magmatic in origin.

The magmatic origin for Nb- and Ta-oxide minerals has been pointed out by both experimental studies and natural examples of rare-element mineralizations related to peraluminous granites and granitic pegmatites (e.g. Cuney et al., 1992; Keppler, 1993; Linnen, 1998; Linnen and Cuney, 2005; Linnen and Keppler, 1997). Chemical variations of zoned cassiterite and CGM include Ta enrichment towards the rims of some grains. This fact is in accordance with the differences in solubility for Nb and Ta in peraluminous melts, so that fractional crystallization would have led to a segregation of progressively Ta-Nb-Sn-rich evolved melts, with less viscosity and density and lower temperature upwards, thus increasing diffusion rates of incompatible rare elements such as Nb and Ta and permitting late liquid-liquid ultrafractionation of granitic melts (Hannah and Stein, 1990). Thus, concentration of those rare elements and volatiles is high enough to promote primary crystallization of CGM as well as cassiterite progressively enriched in Ta (Cuney et al., 1985; Linnen and Cuney, 2005; Linnen and Keppler, 1997).

6.1.1. Cassiterite

Ta# ratios of most cassiterite crystals are greater than 0.5 (Figs. 10a, 11), which is expected from the partition coefficients for Ta and Nb in

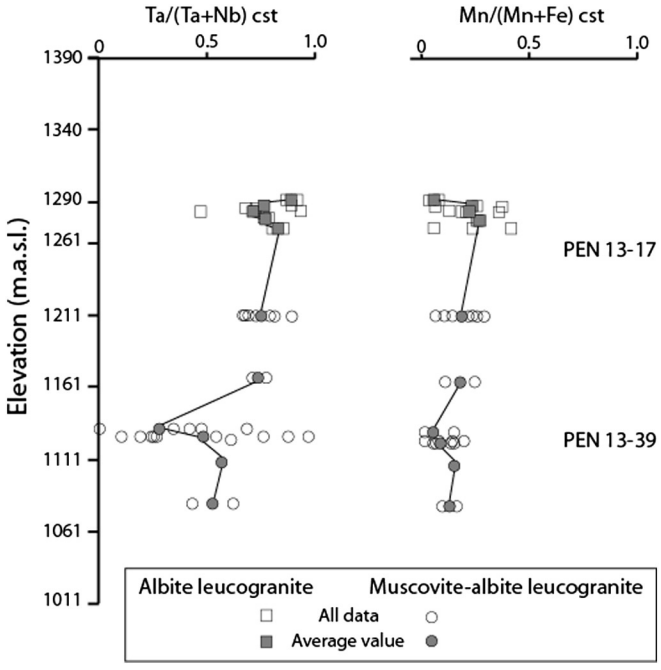

Fig. 11. Evolution of Ta# and Mn# ratios for cassiterite from the muscovite-albite leucogranite to the albite leucogranite in holes Pen 13–17 and Pen 13–39, represented in the same vertical line at their real elevation. As there is a wide range of values, average data has also been plotted for each sample.

this mineral (Černý and Ercit, 1985, 1989). The muscovite-albite leucogranite shows higher Nb-Ta fractionation in cassiterite than the albite-rich facies, which would suggest a crystallization by local supersaturation of the former, possibly favored by supercooling or boundary layer effect (London, 2008, 2009). This supersaturation effect would have decreased upwards during crystallization of the albite leucogranite, as suggested by narrowing of Nb-Ta fractionation. Similar Ta_2O_5 contents have been reported in cassiterite deposited in granites from the Cinovec cupola (Rub et al., 1998), Podlesí (Breiter et al., 2007), Songuhugang (Zhu et al., 2015) and Ponte Segade, in Spain (Canosa et al., 2012). It has also been noticed a clear preference to incorporate Fe instead of Mn in this mineral, which can be the consequence of competence with other magmatic minerals regarding Mn, as is the case of spessartine and Nb-Ta-oxides, and would support the magmatic origin for cassiterite. Comparable high FeO contents have also been observed in other magmatic cassiterites reported in topaz-bearing rapakiwi granites from Finland (Haapala, 1997) and the Pitinga albite-bearing granite in Brazil (Costi et al., 2009). These elements enter in the cassiterite structure by means of ideal coupled substitution $3Sn^{4+} \leftrightarrow (Fe,Mn)^{2+} + 2(Nb,Ta)^{5+}$ (Figs. 10b,c), which is a common and widespread scheme in similar ore deposits from highly peraluminous granites, LCT pegmatites and hydrothermal quartz veins (Černý and Ercit, 1985; Černý et al., 1985a; Chicharro et al., 2015; Llorens and Moro, 2012a,b; Neiva, 1996; Pal et al., 2007; Spilde and Shearer, 1992).

6.1.2. Ta-Nb-oxides

Regular disseminations of CGM throughout the Penouta leucogranite, as well as normal and oscillatory zoning of most grains, is strong argument for a magmatic origin of these minerals from evolved silicate melts (Černý et al., 1985a; Lahti, 1987; Tindle and Breaks, 2000). The normal zoning responds to fractionation patterns of decreasing Nb/Ta ratios from core to rim, as in the case of cassiterite. In this sense, trend I observed in Fig. 12a responds to a normal evolution of CGM in granites and pegmatites worldwide (e.g. Abdalla et al., 1998; Beurlen et al., 2008; Černý et al., 1986, Melcher et al., 2015; René and Škoda, 2011) and is in line with a melt evolution upwards from the muscovite-albite leucogranite of the Penouta deposit, containing low grade mineralization (western and bottom zones), to the most evolved albite leucogranite and BPA, enriched in Sn, Ta and Nb (eastern top zones). Moreover, the substitution scheme $(Fe,Mn)^{2+} + 2(Nb,Ta)^{5+} \leftrightarrow 3(Ti,Sn)^{4+}$ (Černý and Ercit, 1985; Černý et al., 1985b) also endorses the magmatic origin of the CGM of the Penouta leucogranite.

In contrast, trend II reflects high Nb/Ta fractionation in both facies of the leucogranite (muscovite-albite and albite leucogranite, see Fig. 12a) and BPA due to local supersaturation effects during crystallization (London, 2008, 2009, 2014). This process is more evident in the BPA

Table 4
Representative compositions of columbite-group minerals from the Penouta leucogranite facies, BPA and greisen (wt.%) with their structural formulae (apfu).

	Muscovite-albite leucogranite				Albite leucogranite						Grt-rich aplite	BPA		Greisen
	clf	clf	clm	clm	clf	clm	clm	clm	tnm	tnm	clf	clm	tnm	tnm
Nb_2O_5 (wt.%)	57.31	42.59	60.92	55.31	33.31	59.90	33.10	61.46	23.22	20.05	46.35	37.61	27.39	19.17
Ta_2O_5	22.43	38.43	19.70	25.84	48.93	20.30	48.27	19.02	59.49	64.03	34.82	44.63	56.21	65.24
TiO_2	0.07	0.01	0.02	0.01	0.96	0.02	0.55	0.05	0.02	0.11	0.11	0.46	0.13	0.00
SnO_2	0.11	0.07	0.07	0.00	0.30	0.07	0.49	0.01	0.13	0.13	0.02	0.14	0.14	0.03
UO_2	0.00	0.00	0.01	0.00	0.00	0.00	0.34	0.00	0.00	0.00	0.00	0.01	0.00	0.00
FeO	13.60	12.39	5.23	3.19	9.87	3.51	2.52	7.76	3.12	1.97	12.44	6.90	7.71	1.99
MnO	5.82	7.14	14.63	15.98	6.93	15.92	14.54	12.25	13.80	14.21	6.26	10.57	8.80	14.05
CaO	0.00	0.02	0.03	0.02	0.02	0.01	0.02	0.02	0.04	0.01	0.02	0.02	0.01	0.04
Na_2O	0.00	0.04	0.01	0.00	0.00	0.02	0.01	0.00	0.00	0.00	0.01	0.00	0.00	0.00
Total	99.33	100.71	100.62	100.35	100.31	99.74	99.83	100.57	99.82	100.50	100.01	100.34	100.38	100.52
Structural formulae calculated on the basis of O = 6														
Nb (apfu)	1.611	1.272	1.667	1.558	1.042	1.657	1.044	1.678	0.776	0.679	1.367	1.154	0.891	0.653
Ta	0.379	0.691	0.324	0.438	0.921	0.338	0.916	0.312	1.196	1.304	0.618	0.824	1.100	1.336
Ti	0.003	0.001	0.001	0.000	0.050	0.001	0.029	0.002	0.001	0.006	0.005	0.023	0.007	0.000
Sn	0.003	0.002	0.002	0.000	0.008	0.002	0.014	0.000	0.004	0.004	0.000	0.004	0.004	0.001
ΣB site	1.996	1.965	1.994	1.996	2.020	1.998	2.003	1.993	1.977	1.992	1.991	2.005	2.002	1.990
U	0.000	0.000	0.000	0.000	0.000	0.000	0.005	0.000	0.000	0.000	0.000	0.000	0.000	0.000
Fe	0.707	0.685	0.265	0.166	0.571	0.180	0.147	0.392	0.193	0.123	0.679	0.392	0.464	0.125
Mn	0.307	0.400	0.750	0.843	0.406	0.825	0.859	0.627	0.864	0.901	0.346	0.608	0.536	0.896
Ca	0.000	0.002	0.002	0.001	0.002	0.001	0.002	0.002	0.003	0.001	0.001	0.002	0.000	0.003
Na	0.000	0.005	0.002	0.000	0.000	0.002	0.001	0.000	0.000	0.000	0.001	0.000	0.000	0.000
ΣA site	1.014	1.091	1.018	1.010	0.978	1.008	1.014	1.020	1.060	1.025	1.027	1.001	1.001	1.025
Mn/(Mn + Fe)	0.302	0.369	0.739	0.835	0.416	0.821	0.854	0.615	0.817	0.880	0.338	0.608	0.536	0.877
Ta/(Ta + Nb)	0.191	0.352	0.163	0.219	0.469	0.169	0.467	0.157	0.606	0.658	0.311	0.417	0.552	0.672

clm: columbite-Mn; clf: columbite-Fe; tnm: tantalite-Mn.

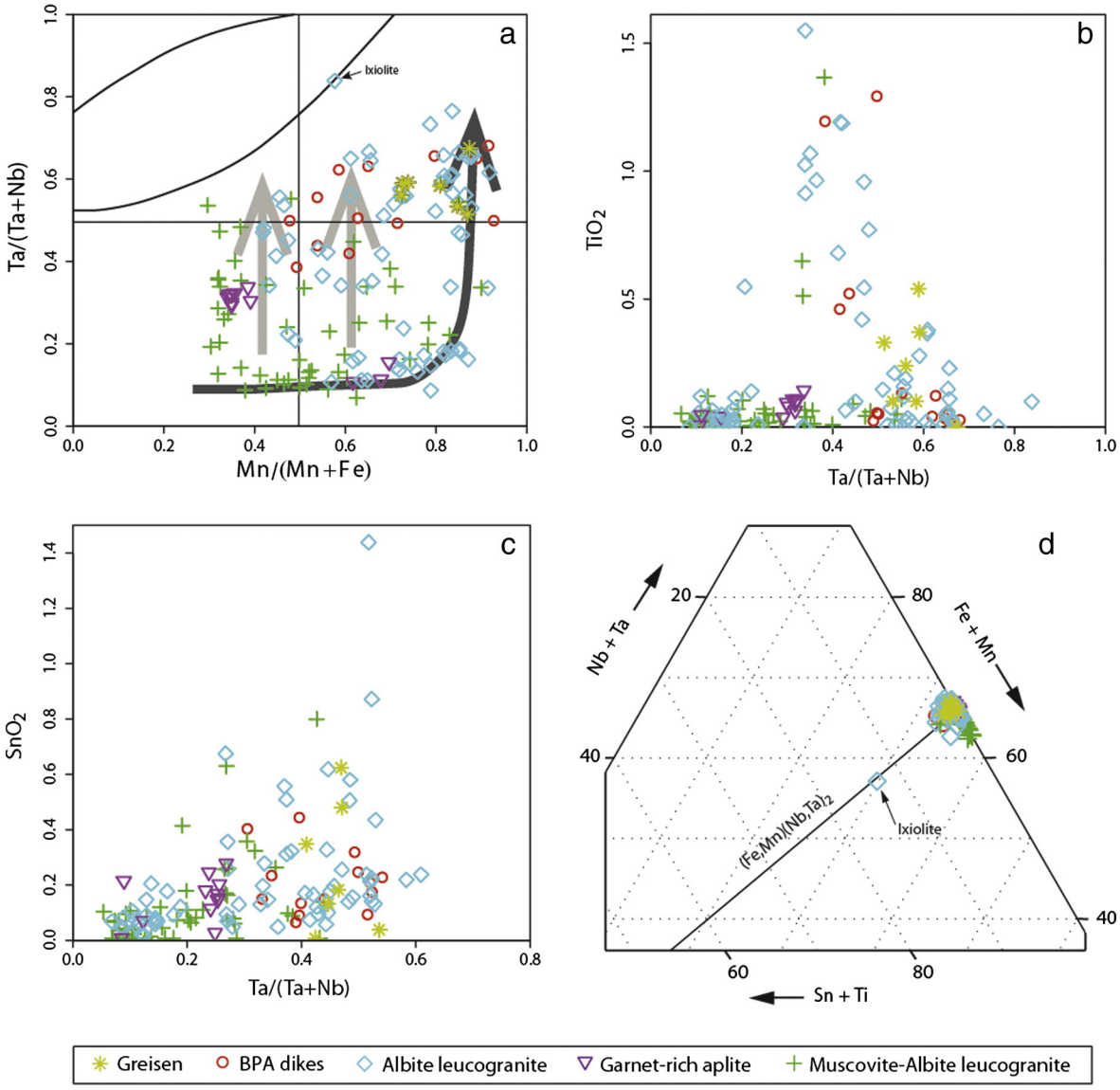

Fig. 12. a) CGM data plotted in the columbite quadrilateral. Two trends can be differentiated: trend I along the dark grey arrow, which responds to the normal evolution of CGM from muscovite-albite leucogranite to albite leucogranite and BPA to the top of the deposit; and trend II corresponding with Ta-enriched compositions along the light grey arrows, which is interpreted as local supersaturation of the melt causing complex oscillatory and patchy zoning of CGM crystals; b) TiO_2 (wt.%) *vs.* Ta# in CGM, showing slight negative correlation in some albite leucogranite samples; c) SnO_2 (wt.%) *vs.* Ta# in CGM, showing a broad positive correlation; d) CGM analyses plotted in the Sn + Ti–Nb + Ta–Fe + Mn triangular diagram, displaying limited variation along the Nb + Ta–Fe + Mn border.

from the top of the deposit, where the local saturation in the boundary layer liquid due to pile-up of excluded components, would have given rise to the alternation of aplite and pegmatite layers as well as the oscillation between albite- and quartz-rich zones in the BPA bodies. The same model could be translated to the crystalline scale and thus reflected in the common complex oscillatory zoning observed in most CGM of the Penouta deposit. The occurrence of oscillatory zoning is also commonly related to local fluctuations in the composition of the mineral-forming melt or fluid under near-equilibrium conditions, as a result of magmas mixing, rapid cooling or degassing/decompression of the igneous system, thus incorporating Nb/Ta and Fe/Mn in different rates (Holten et al., 1997; Shore and Fowler, 1996). This zoning pattern is very common in CGM from similar granite and pegmatite deposits (e.g. Anderson et al., 2013; Badanina et al., 2015; Llorens and Moro, 2012a; Tindle and Breaks, 2000; Van Lichtervelde et al., 2007).

Regarding the slight reverse trend in the Ta# ratio observed in Fig. 13 for the CGM deposited in the muscovite-albite leucogranite from bottom to top, complex compositional zoning makes difficult to distinguish possible late replacing features from primary ones. This zoning scheme suggests overprinting of original patterns during late-magmatic to subsolidus dissolution-reprecipitation processes, as well as late low temperature alterations, as in the case of microlite crystallization (Černý et al., 1986). In this sense, it is noticeable the presence of numerous veinlets crosscutting the upper part of the granite, commonly filled by late quartz and pyrite, together or not with clays, and the presence of a sulphide assemblage disseminated in the granite (sphalerite, pyrite, molybdenite).

No CGM have been observed in the hydrothermal quartz veins, and those identified in the greisen zones seem to be the result of original Nb-Ta oxides partially altered and corroded, so that they remain in the greisen rocks as relicts of the original crystals formed in the Penouta granite during the magmatic stage. Absence of typical textures originated by fluids in the CGM (e.g. veinlets or late infillings of previous cracks in CGM) also points to a low influence of those hydrothermal fluids in dissolution and recrystallization processes of the primary oxides. It is also suggested by the low Ti contents both in cassiterite and in CGM.

This is in accordance with the results of fluid inclusions studied by Mangas and Arribas (1987) in several Variscan Sn-bearing deposits

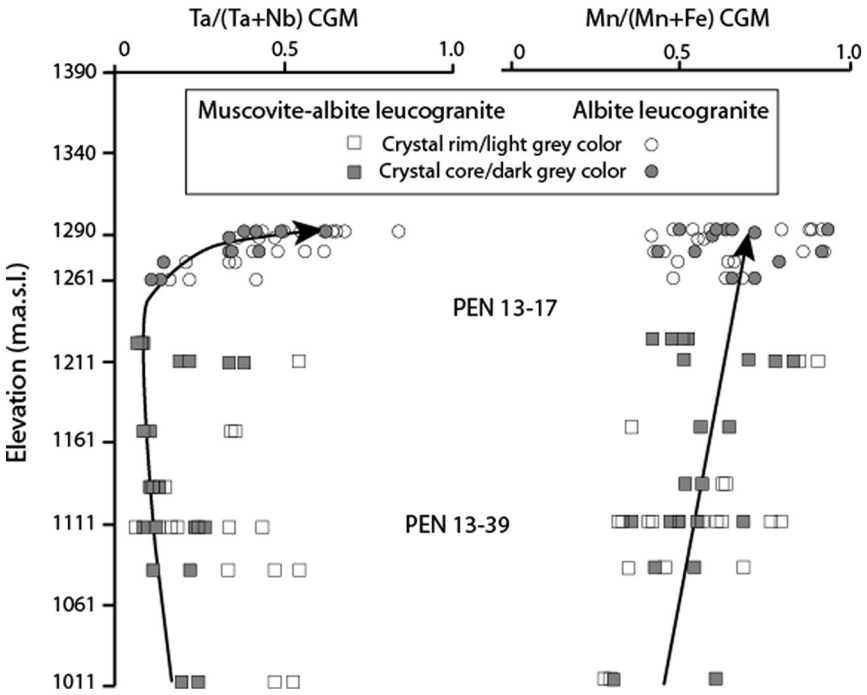

Fig. 13. Evolution of Ta# and Mn# ratios for CGM (cores and rims) from the muscovite-albite leucogranite to the albite leucogranite in holes Pen 13–17 and Pen 13–39, represented in the same vertical line at their real elevation.

from western Spain, where Penouta samples were investigated. They concluded that early fluids would be related with a magmatic origin, thus crystallizing CGM and cassiterite directly from the melt, and only at the end of the mineralizing processes the magmatic fluid would have mixed with metamorphic and meteoric waters, then giving rise to mineralization of cassiterite in the greisen and quartz veins.

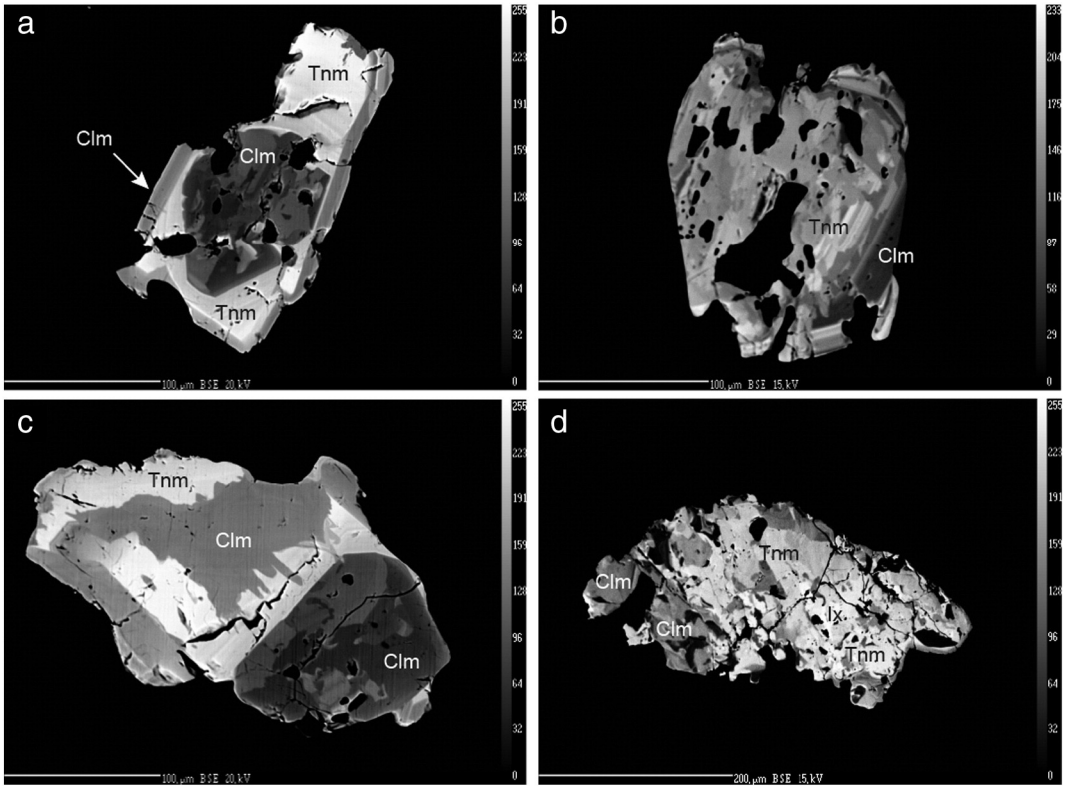

Fig. 14. BSE images of zoned CGM: a) CGM with reverse zoning from corroded columbite-Mn core towards tantalite-Mn, afterwards surrounded by a Nb-rich rim; b) CGM with a complex zoning pattern, patchy to truncated oscillatory zoning and reverse zoning towards some rims; c) Complex zoning of a CGM, showing a partially corroded Nb-rich core surrounded by Ta-rich patches. Relicts of columbite-Mn remain after coating by tantalite-Mn; d) CGM showing complex patchy zoning and ixiolite relicts. Cst: cassiterite, Clf: columbite-Fe, Clm: columbite-Mn, Tnm: tantalite-Mn, Ix: ixiolite.

6.2. Factors controlling Nb-Ta fractionation

Fractional crystallization is the most common explanation invoked for increasing Ta trends towards the upper part of the granite cupolas and throughout pegmatite fields from less to more evolved bodies, and even at the level of individual grains attending to internal compositional zoning (Beurlen et al., 2008; Tindle et al., 1998). Concentration of fluxing elements, such as Li, P, F or B, has an effect on the tantalite solubility as they reduce viscosity of the melt and permit accumulation of high field strength elements towards the upper zone of a magmatic chamber (Bartels et al., 2010, 2011).

In addition, fluorine enhances solubility of tantalite more than columbite at moderate temperatures, and reduces pH of the mineral-forming environment, facilitating late precipitation of Ta-rich phases (Alexandrov et al., 1985). Thus, the previously described reverse zoning showed by Nb in some CGM of the Penouta leucogranite (Fig. 14a,b) could be interpreted as the result of disequilibrium between the growing crystal and the host fluids due to sudden changes in pH or temperature, as reported in similar deposits from Egypt (Abdalla et al., 1998).

In the case of the Penouta Li- and P-poor leucogranite, elevated activity of F throughout the crystallization process is evident from increasing F contents in minerals such as fluorapatite (up to 3.21 wt.%), muscovite (up to 1.10 wt.%), and the presence of fluorite in the cupola, although the overall volume of these minerals is very low relative to major minerals forming the Penouta granite, such as quartz and feldspars. Attending to fluorine content of apatite vertically in the drill holes, it reflects the same behavior than Ta, which could be in line with the influence of F in the solubility and mobility of this metal.

Moreover, the Penouta granite display increasing amount of albite towards the upper part of the deposit, as a consequence of Na- and Al-enrichment of the melt in contrast to decreasing SiO_2 contents, which would be consistent with increasing F towards the cupola (Manning, 1981). This fact points again to the important role of fluxing elements such as F in the evolution of such highly evolved melts, as occurs in similar granite systems of Egypt (Abdalla et al., 1998; Helba et al., 1997), Beauvoir (Raimbault et al., 1995), Yichun (Huang et al., 2002), Thailand (Pollard et al., 1995), Podlesí (Breiter et al., 2007) and Navasfrías, in Spain (Llorens and Moro, 2012a,b).

According to that, fluorine would have remained during consolidation of the granite until late magmatic stages, which could have led to increase differences between Nb- and Ta- solubility and controlling precipitation of Ta-rich compounds late in the paragenesis, as they are more stable at lower temperatures (Wang et al., 1982). The increase of fluxing elements such as F in the residual melt could have raise the Ta/Nb ratio, causing resorption of earlier Nb-rich crystals, as suggested by backscattered images of several CGM, where corroded cores are observed (Fig. 9d, 14a,c). This corrosion together with the connection of zoning with peripheral zones of the grain and high variations of Ta# and Mn# ratios, could be in keeping with a late- to post-magmatic supercritical vapor phase causing the zoning patterns observed in the Penouta leucogranite.

Recent experimental studies suggested that F concentration would have no influence on the columbite and tantalite solubilities in nearly fluid-saturated granitic melts (Aseri et al., 2015; Fiege et al., 2011). These authors suggest that solubility is mainly controlled by temperature and ASI of the melts, so that the solubility products increase with increasing ASI in peraluminous melts (Van Lichtervelde et al., 2010). However, in the Penouta granite, where influence of Li, P and B is negligible and highest ASI values correspond with the less evolved samples of the muscovite-albite leucogranite, and consequently the less Ta-enriched of the deposit, F seems to be the most probable factor controlling Nb and Ta crystallization.

Moreover, taking into account the evolution of the leucogranite from muscovite-albite to albite-rich facies towards the apical zones, the fractionation of micas could have led to the same effect that fluorine, as white mica could have yield enrichment in Ta relative to Nb upwards in the granite body by the differences in the partition coefficients of both elements (Stepanov et al., 2014). In this way, the combination of white mica fractionation, as mechanism to increase the Ta/Nb ratio upwards, together with the fluorine enrichment in the apical zones, which extends the crystal fractionation process in time, could explain the Ta enrichment of the melt and the zoning patterns of CGM observed in the apical zone.

The same process could be applied for the important variation in Mn# observed in CGM (Fig. 12a), so that fluctuations in the Fe and Mn activities in the forming-melt could be explained by competition with other Fe- and Mn-bearing minerals in the paragenesis, as the phengitic mica, as abundant mineral but with low contents in Mn, although spessartine and apatite could have played a similar role as scarce but Mn-rich phases in the Penouta leucogranite, these minerals being capable of scavenging Fe and Mn in the paragenesis. This behavior has been observed in other deposits, especially in LCT pegmatites such as those related to the Jálama batholith, in Spain (Llorens and Moro, 2010, 2012a), Kolmozero, in Russia (Badanina et al., 2015), the Piława Górna deposit, in Poland (Pieczka et al., 2013), Kenticha, in Ethiopia (Küster, 2009), the Pampean Ranges, Argentina (Galliski and Černý, 2006), the Eräjärvi area, in Finland (Lahti, 1987) or the Barroso-Alvão field, in Portugal (Martins et al., 2011).

7. Conclusions

The Sn-Ta-Nb Penouta deposit mainly consists of a peraluminous, highly evolved rare-metal leucogranite, where BPA dikes were developed irregularly towards the eastern zone of the granitic cupola during a late-magmatic stage. A subsequent hydrothermal event triggered a strong greisenization of the upper part of the granitic cupola and the hosting metamorphic rocks, giving rise to the crystallization of a stockwork of quartz veins.

Mineralization consists of cassiterite I and CGM finely disseminated from the western muscovite-albite leucogranite to the eastern albite leucogranite and the BPA. Their textural and chemical features support the magmatic origin for both minerals, although cassiterite I crystallized slightly later in the sequence. Additionally, coarse-grained cassiterite II crystallized restricted to the greisen zone and the quartz veins towards the eastern cupola zone of the leucogranite, so that related to a later hydrothermal event, whereas CGM only appears in the greisen as relicts of alteration of the magmatic oxides.

Chemical composition of CGM reveals two evolutionary trends: trend I evolves from columbite-Fe in the muscovite-albite leucogranite to tantalite-Mn towards the albite leucogranite and BPA, reflecting high Fe/Mn fractionation followed by Nb/Ta fractionation of the melt from west to east of the deposit, where the cupola effect is better represented. This feature is typical of highly evolved rare-element granites and pegmatites worldwide; trend II shows a strong Ta enrichment of the CGM, mainly those with complex oscillatory zoning patterns. These variations are also reflected by cassiterite I and II, which are chemically very similar.

High Ta-Nb and Mn-Fe fluctuations in the melt are suggested to explain such variations, usually caused by increasing Ta and Mn contents as fractionation occurs, as well as by competition with other Fe-Mn-bearing minerals such as garnet or muscovite. Considering that other fluxing elements than F had a limited role in the evolution of the deposit and mineralization, enhancement of fluorine activity upwards could have led to Ta-enrichment of the residual melt relative to Nb, thus concentrating in the last crystallization stages of the granite. Nevertheless, the fractionation of white mica could also result in a Ta enrichment in the melt upwards and the zoning pattern observed in CGM and cassiterite.

Acknowledgments

We gratefully acknowledge P. Uher and anonymous reviewers for their critical comments that have considerably improved the original

manuscript. The authors thank for technical and human support provided by SGIker of UPV/EHU and European funding (ERDF and ESF). Thanks are due to M.A. Fernández for performing many electron-microprobe analyses and providing BSE images as well as general assistance during the analytical work. The authors sincerely thank the work team of Strategic Minerals Spain for supporting in the field work and improvement of the manuscript. This study was financially supported by Strategic Minerals Spain S.L. and the Torres Quevedo Program (PTQ-12-05703), and was developed in collaboration with the University of Salamanca by means of a research project.

References

Abdalla, H.M., Helba, H.A., Mohamed, F.H., 1998. Chemistry of columbite-tantalite minerals in rare metal granitoids, Eastern Desert. Egypt. Mineral. Mag. 62:821–836. http://dx.doi.org/10.1180/002646198548197.

ADARO, 1982. Proyecto de Investigación de la Mina de Penouta. Cálculo de reservas para leyes de corte de 800 y 600 g/t. Informe Interno, Madrid (69 pp. (Unpubl.).

ADARO, 1985. Investigación Minera del Yacimiento de Penouta. 9 volumes. Informe Interno, Madrid (Unpubl.).

Alexandrov, I.V., Krasov, A.M., Kochnova, L.N., 1985. The effects of K, Na and F on rock-forming mineral assemblages and the formation of tantalo-niobate mineralization in rare-element granite pegmatites. Geochem. Int. 22, 85–92.

Anderson, M.O., Lentz, D.R., McFarlane, C.R.M., Falck, H., 2013. A geological, geochemical and textural study of a LCT pegmatite: implications for the magmatic versus metasomatic origin of Nb–Ta mineralization in the Moose II pegmatite, Northwest Territories. Canada. J. Geosci. 58:299–320. http://dx.doi.org/10.3190/jgeosci.149.

Arribas, A., Gonzalo, F., Iglesias, M., 1982. Génesis de una mineralización asociada a una cúpula granítica: el yacimiento de estaño de Golpejas (Salamanca). Cuad. Lab. Xeolóx. Laxe 3, 563–592 84-7492-149-X.

Aseri, A.A., Linnen, R.L., Che, X.Z., Yves, R., Francois, H., 2015. Effects of fluorine on the solubilities of Nb, Ta, Zr and Hf minerals in highly fluxed water-saturated haplogranitic melts. Ore Geol. Rev. 64:736–746. http://dx.doi.org/10.1016/j.oregeorev.2014.02.014.

Badanina, E.V., Veksler, I.V., Thomas, R., Syritso, L.F., Trumbull, R.B., 2004. Magmatic evolution of Li-F, rare-metal granites: a case study of melt inclusions in the Khangilay complex, Eastern Transbaikalia (Russia). Chem. Geol. 210:113–133. http://dx.doi.org/10.2113/gscanmin.44.3.667.

Badanina, E.V., Sitnikova, M.A., Gordienko, V.V., Melcher, F., Gäbler, H.-E., Lodziak, J., Syritso, L.F., 2015. Mineral chemistry of columbite–tantalite from spodumene pegmatites of Kolmozero, Kola Peninsula (Russia). Ore Geol. Rev. 64:720–735. http://dx.doi.org/10.1016/j.oregeorev.2014.05.009.

Bartels, A., Holtz, F., Linnen, R.L., 2010. Solubility of manganotantalite and manganocolumbite in pegmatitic melts. Am. Mineral. 95:537–544. http://dx.doi.org/10.2138/am.2010.3157.

Bartels, A., Vetere, F., Holtz, F., Behrens, H., Linnen, R.L., 2011. Viscosity of flux-rich pegmatitic melts. Contrib. Mineral. Petrol. 162:51–60. http://dx.doi.org/10.1007/s00410-010-0582-3.

Beurlen, H., Da Silva, M.R.R., Thomas, R., Soares, D.R., Olivier, P., 2008. Nb-Ta-(Ti-Sn) oxide mineral chemistry as tracer of rare-element granitic pegmatite fractionation in the Borborema Province, Northeastern Brazil. Mineral. Deposita 43:207–228. http://dx.doi.org/10.1007/s00126-007-0152-4.

Boyd, R., 2012. The EU potential critical minerals resource. Critical minerals for the clean energy and high technology industries 2012 and beyond – the EU perspective. May 21 2012. Geological Survey of Denmark and Greenland, Øster Voldgade 10, Copenhagen.

Breiter, K., Škoda, R., Uher, P., 2007. Nb-Ta-Ti-W-Sn-oxide minerals as indicators of peraluminous P- and F-rich granitic system evolution: Podlesí, Czech Republic. Mineral. Petrol. 91:225–248. http://dx.doi.org/10.1007/s00710-007-0197-1.

Canosa, F., Martín-Izard, A., Fuertes-Fuente, M., 2012. Evolved granitic system as a source of rare-element deposits: The Ponte Segade case (Galicia, NW Spain). Lithos 153: 165–176. http://dx.doi.org/10.1016/j.lithos.2012.06.029.

Černý, P., Ercit, S., 1985. Some recent advances in the mineralogy and geochemistry of Nb and Ta in rare-element granitic pegmatites. Bull. Mineral. 108, 499–532.

Černý, P., Ercit, S., 1989. Mineralogy of niobium and tantalum: crystal chemical relationships, paragenetic aspects and their economic implications. In: Möller, P., Černý, P., Saupé, F. (Eds.), Lanthanides, Tantalum and Niobium. Springer-Verlag, New York:pp. 27–29 http://dx.doi.org/10.1007/978-3-642-87262-4 (SGA Special Publications 7).

Černý, P., Meintzer, R.E., Anderson, A.J., 1985a. Extreme fractionation in rare-element granitic pegmatites: selected examples of data and mechanisms. Can. Mineral. 23, 381–421.

Černý, P., Roberts, W.L., Ercit, T.S., Chapman, R., 1985b. Wodginite and associated minerals from the Peerless pegmatite, Pennington County, South Dakota. Am. Mineral. 70, 1044–1049.

Černý, P., Goad, B.E., Hawthorne, C., Chapman, R., 1986. Fractionation trends of the Nb- and Ta-bearing oxide minerals in the Greer Lake pegmatitic granite and its pegmatite aureole, southeastern Manitoba. Am. Mineral. 71, 501–517.

Černý, P., Ercit, T.S., Vanstone, P.T., 1996. Petrology and mineralization of the Tanco rare-element pegmatite, Southeastern Manitoba - Field Trip A3. Geological Association of Canada/Mineralogical Association of Canada Annual Meeting, Winnipeg, Manitoba May 27–29, 1996. (72 pp.).

Charoy, B., Noronha, F., 1996. Multistage growth of a rare-element, volatile-rich microgranite at Argemela (Portugal). J. Petrol. 37:73–94. http://dx.doi.org/10.1093/petrology/37.1.

Chicharro, E., Martín-Crespo, T., Gómez-Ortiz, D., López-García, J.A., Oyarzun, R., Villaseca, C., 2015. Geology and gravity modeling of the Logrosán Sn–(W) ore deposits (Central Iberian Zone, Spain). Ore Geol. Rev. 65:294–307. http://dx.doi.org/10.1016/j.oregeorev.2014.10.005.

Chudík, P., Uher, P., Kohút, M., Bačík, P., 2008. Accessory columbite to tantalite, tapiolite and zircon: products of extreme fractionation in highly peraluminous pegmatitic granite from the Považský Inovec Mountains, Western Carpathians, Slovakia. J. Geosci. 53:323–334. http://dx.doi.org/10.3190/jgeosci.031.

Costi, H.T., Dall'agnol, R., Pichavant, M., Rämö, O.T., 2009. The peralkaline tin-mineralized Madeira cryolite albite-rich granite of Pitinga, Amazonian craton, Brazil: petrography, mineralogy and crystallization processes. Can. Mineral. 47:1301–1327. http://dx.doi.org/10.3749/canmin.47.6.1301.

Cuney, M., Autran, A., Burnol, L., 1985. Premiers resultats par le sondage GPF de 900 m realize sur le granite sodo-litique et fluore a mineralization disseminee de Beavour. Chron. Rech. Mineral. 481, 59–63.

Cuney, M., Marignac, C., Weisbrod, A., 1992. The Beauvoir topaz-lepidolite albite granite (Massif Central, France); the disseminated magmatic Sn-Li-Ta-Nb-Be mineralization. Econ. Geol. 87:1766–1794. http://dx.doi.org/10.2113/gsecongeo.87.7.1766.

Díez Montes, A., 2006. La Geología del Dominio "Ollo de Sapo" en las comarcas de Sanabria y Terra do Bolo. Universidad de Salamanca e Instituto Geológico y Minero de España, Tesis Doctoral (496 pp.).

Díez Montes, A., Martínez Catalán, J.R., Bellido Mulas, F., 2010. Role of the Ollo de Sapo massive felsic volcanism of NW Iberia in the Early Ordovician dynamics of northern Gondwana. Gondwana Res. 17:363–376. http://dx.doi.org/10.1016/j.gr.2009.09.001.

Fetherston, J.M., 2004. Tantalum in Western Australia: Western Australia Geological Survey. Mineral Resources Bulletin 22 162 p..

Fiege, A., Kirchner, C., Holtz, F., Linnen, R.L., Dziony, W., 2011. Influence of fluorine on the solubility of manganotantalite ($MnTa_2O_6$) and manganocolumbite ($MnNb_2O_6$) in granitic melts - an experimental study. Lithos 122:165–174. http://dx.doi.org/10.1016/j.lithos.2010.12.012.

Galliski, M.A., Černý, P., 2006. Geochemistry and structural state of columbite-group minerals in granitic pegmatites of the Pampean Ranges. Argentina. Can. Mineral. 44: 645–666. http://dx.doi.org/10.2113/gscanmin.44.3.

García Guinea, J., Martínez Frías, J., 1992. Recursos minerales de España. CSIC, Madrid 1448 pp.

González-Clavijo, E., Díez Balda, M.A., Álvarez, F., 1993. Structural study of a semiductile strike-slip system in the Central Iberian Zone (Variscan Fold Belt, Spain): structural controls in gold deposits. Geol. Rundsch. 82:448–460. http://dx.doi.org/10.1007/BF00212409.

Gonzalo, F.J., Gracia, A.S., 1985. Yacimientos de estaño del oeste de España: Ensayo de caracterización y clasificación económicas. Cuad. Lab. Xeolóx. Laxe 9, 265–303.

Haapala, I., 1997. Magmatic and postmagmatic processes in tin-mineralized granites: topaz-bearing leucogranite in the Eurajoki rapakivi granite stock. Finland. J. Petrol. 38:1645–1659. http://dx.doi.org/10.1093/petroj/38.12.

Hannah, J.L., Stein, H.J., 1990. Magmatic and hydrothermal processes in ore-bearing systems. In: Stein, H., Hannah, J. (Eds.), Ore-bearing Granite Systems; Petrogenesis and Mineralizing Processes. 246, pp. 1–11 Geol. Soc. Amer. Spec. Paper. 0813722462, 9780813722467.

Hawthorne, F.C., Henry, D.J., 1999. Classification of the minerals of the tourmaline group. Eur. J. Mineral. 11, 201–215.

Helba, H., Trumbull, R.b., Morteani, G., Khalil, S.O., Arslan, A., 1997. Geochemical and petrographic studies of Ta mineralization in the Nuweibi albite granite complex, Eastern Desert. Egypt. Miner. Deposita 32:164–179. http://dx.doi.org/10.1007/s001260050082.

Henry, D.J., Guidotti, C.V., 1985. Tourmaline as a petrogenetic indicator mineral: an example from the staurolite-grade metapelites of NW Maine. Am. Mineral. 70, 1–15.

Henry, D.J., Novák, M., Hawthorne, F.C., Ertl, A., Dutrow, B.L., Uher, P., Pezzotta, F., 2011. Nomenclature of the tourmaline-supergroup minerals. Am. Mineral. 96:895–913. http://dx.doi.org/10.2138/am.2011.3636.

Holten, T., Jamtveit, B., Meakin, P., Cortini, M., Blundy, J., Austrheim, H., 1997. Statistical characteristics and origin of oscillatory zoning in crystal. Am. Mineral. 82, 596–606.

Huang, X.L., Wang, R.C., Chen, X.M., Hu, H., Liu, C.S., 2002. Vertical variations in the mineralogy of the Yichun topaz-lepidolite granite, Jiangxi province, Southern China. Can. Mineral. 40:1047–1068. http://dx.doi.org/10.2113/gscanmin.40.4.

Janoušek, V., Farrow, C.M., Erban, V., 2006. Interpretation of whole-rock geochemical data in igneous geochemistry: introducing Geochemical Data Toolkit (GCDkit). J. Petrol. 47:1255–1259. http://dx.doi.org/10.1093/petrology/egl013.

Keppler, H., 1993. Influence of fluorine on the enrichment of high field strength trace elements in granitic rocks. Contrib. Mineral. Petrol. 114:479–488. http://dx.doi.org/10.1007/BF00321752.

Küster, D., 2009. Granitoid-hosted Ta mineralization in the Arabian–Nubian Shield: ore deposit types, tectono-metallogenetic setting and petrogenetic framework. Ore Geol. Rev. 35:68–86. http://dx.doi.org/10.1016/j.oregeorev.2008.09.008.

Lahti, S.I., 1987. Zoning in columbite–tantalite crystals from the granitic pegmatites of the Eräjärvi area, southern Finland. Geochim. Cosmochim. Acta 51:509–517. http://dx.doi.org/10.1016/0016-7037(87)90065-2.

Linnen, R.L., 1998. The solubility of Nb-Ta-Zr-Hf-W in granitic melts with Li and Li + F; constraints for mineralization in rare metal granites and pegmatites. Econ. Geol. 93: 1013–1025. http://dx.doi.org/10.2113/gsecongeo.93.7.1013.

Linnen, R.L., Cuney, M., 2005. Granite-related rare-element deposits and experimental constraints on Ta-Nb-W-Sn-Zr-Hf mineralization. In: RL, L., IM, S. (Eds.), Rare Element Geochemistry and Mineral DepositsGeological Association of Canada Short Course

Notes 17. Geological Association of Canada, St. John's, NL:pp. 45–68. http://dx.doi.org/10.2113/gsecongeo.101.4.904.
Linnen, R.L., Keppler, H., 1997. Columbite stability in granitic melts: consequences for the enrichment and fractionation of Nb and Ta in the Earth crust. Contrib. Mineral. Petrol. 128:213–227. http://dx.doi.org/10.1007/s004100050304.
Llorens, T., Moro, M.C., 2010. Microlite and tantalite in the LCT granitic pegmatites of La Canalita, Navasfrías Sn-W District, Salamanca, Spain. Can. Mineral. 48:549–564. http://dx.doi.org/10.3749/canmin.48.2.375.
Llorens, T., Moro, M.C., 2012a. Oxide minerals in the granitic cupola of the Jálama Batholith, Salamanca, Spain. Part I: accessory Sn, Nb, Ta and Ti minerals in leucogranites, aplites and pegmatites. J. Geosci. 57:25–43. http://dx.doi.org/10.3190/jgeosci.113.
Llorens, T., Moro, M.C., 2012b. Oxide minerals in the granitic cupola of the Jálama Batholith, Salamanca, Spain. Part II: Sn, W and Ti minerals in intra-granitic quartz veins. J. Geosci. 57:155–171. http://dx.doi.org/10.3190/jgeosci.119.
London, D., 2008. Pegmatites. 10. Canadian Mineralogist Special Publication 978-0-921294-47-4 347 pp.
London, D., 2009. The origin of primary textures in granitic pegmatites. Can. Mineral. 47: 697–724. http://dx.doi.org/10.3749/canmin.47.4.
London, D., 2014. A petrologic assessment of internal zonation in granitic pegmatites. Lithos 184-187:74–104. http://dx.doi.org/10.1016/j.lithos.2013.10.025.
López-Moro, F.J., Moro, C., Timón, S.M., Cembranos, M.L., Cózar, J., 2013. Constraints regarding gold deposition in episyenites: the Permian episyenites associated with the Villalcampo Shear Zone, central western Spain. Int. J. Earth Sci. 102:721–744. http://dx.doi.org/10.1007/s00531-012-0844-6.
Mangas, J., Arribas, A., 1987. Fluid inclusion study in different types of tin deposits associated with the Hercynian granites of western Spain. Chem. Geol. 61:193–208. http://dx.doi.org/10.1016/0009-2541(87)90039-8.
Manning, D.A.C., 1981. The effect of fluorine on liquidus phase relationships in the system Qz-Ab-Or with exess water at 1 kb. Contrib. Mineral. Petrol. 76:206–215. http://dx.doi.org/10.1007/BF00371960.
Martins, T., Lima, A., Simmons, S., Falster, A., Noronha, F., 2011. Geochemical fractionation of Nb–Ta oxides in Li-bearing pegmatites from the Barroso–Alvão pegmatite field, Northern Portugal. Can. Mineral. 49:777–791. http://dx.doi.org/10.3749/canmin.49.3.777.
Melcher, F., Graupner, T., Henjes-Kunst, F., Oberthür, T., Sitnikova, M., Gäbler, E., Gerdes, A., Brätz, H., Davis, D., Dewaele, S., 2008. Analytical fingerprint of columbite–tantalite (coltan) mineralization in pegmatites: focus on Africa. Proceed. Ninth Intern. Congr. Appl. Mineral 8–10, 615–624 (ICAM), Brisbane, QLD. September 2008.
Melcher, F., Graupner, T., Gäbler, H.-E., Sitnikova, M., Henjes-Kunst, F., Oberthür, T., Gerdes, A., Dewaele, S., 2015. Tantalum–(niobium–tin) mineralisation in African pegmatites and rare metal granites: constraints from Ta–Nb oxide mineralogy, geochemistry and U–Pb geochronology. Ore Geol. Rev. 64:667–719. http://dx.doi.org/10.1016/j.oregeorev.2013.09.003.
Melcher, F., Graupner, T., Gäbler, H.-E., Sitnikova, M., Oberthür, T., Gerdes, A., Badanina, E., Chudy, T., 2016. Mineralogical and chemical evolution of tantalum–(niobium–tin) mineralisation in pegmatites and granites. Part 2: worldwide examples (excluding Africa) and an overview of global metallogenetic patterns. Ore Geol. Rev. http://dx.doi.org/10.1016/j.oregeorev.2016.03.014 In Press.
Montero, P., Talavera, C., Bea, F., Lodeiro, F.G., Whitehouse, M.J., 2009. Zircon geochronology of the Ollo de Sapo Formation and the age of the Cambro–Ordovician rifting in Iberia. J. Geol. 117:174–191. http://dx.doi.org/10.1086/595017.
Neiva, A.M.R., 1996. Geochemistry of cassiterite and its inclusions and exsolution products from tin and tungsten deposits in Portugal. Can. Mineral. 34:745–768. http://dx.doi.org/10.1016/j.oregeorev.2006.05.013.
Pal, D.C., Mishra, B., Bernhardt, H.-J., 2007. Mineralogy and geochemistry of pegmatite-hosted Sn-, Ta–Nb-, and Zr–Hf-bearing minerals from the southeastern part of the Bastar-Malkangiri pegmatite belt, central India. Ore Geol. Rev. 30:30–55. http://dx.doi.org/10.1016/j.oregeorev.2005.10.004.
Partington, G.A., McNaughton, N.J., Williams, I.S., 1995. A review of the geology, mineralization, and geochronology of the Greenbushes pegmatite, Western Australia. Econ. Geol. 90:616–635. http://dx.doi.org/10.2113/gsecongeo.90.3.616.
Pekov, I.V., 2000. Lovozero massif: History, Pegmatites, Minerals. Ocean Pictures Ltd., Moscow ISBN: 10:5900395278, ISBN-13: 978-5900395272. (480 pp.).
Pereira, E., Ribeiro, A., Meireles, C., 1993. Cisalhamentos hercínicos e controlo das mineralizações de Sn–W, Au e U na Zona Centro-Ibérica, em Portugal. Cuad. Lab. Xeolóx. Laxe 18, 89–119.
Pieczka, A., Szuszkiewicz, A., Szełęg, E., Nejbert, K., Łodziński, M., Ilnicki, S., Turniak, K., Banach, M., Hołub, W., Michałowski, P., Różniak, R., 2013. (Fe, Mn)–(Ti, Sn)–(Nb, Ta) oxide assemblage in a little fractionated portion of a mixed (NYF + LCT) pegmatite from Piława Górna, the Sowie Mts. block, SW Poland. J. Geosci. 58:91–112. http://dx.doi.org/10.3190/jgeosci.136.
Pollard, P.J., Nakapadungrat, S., Taylor, R.G., 1995. The Phuket Supersuite, Southwest Thailand; fractionated I-type granites associated with tin-tantalum mineralization. Econ. Geol. 90:586–602. http://dx.doi.org/10.2113/gsecongeo.90.3.
Pouchour, J.L., Pichoir, F., 1984. A new model for quantitative analysis. I. Application to the analysis of homogeneous samples. La Recherche Aérosp. 3, 13–38.
Pouchour, J.L., Pichoir, F., 1985. "PAP" procedure for improved quantitative microanalysis. Microbeam Anal. 20, 104–105.
Raimbault, L., Cuney, M., Azencott, C., Duthou, J.L., Joron, J.L., 1995. Geochemical evidence for a multistage magmatic genesis of Ta-SnLi mineralization in the granite at Beauvoir, French Massif Central. Econ. Geol. 90:548–596. http://dx.doi.org/10.2113/gsecongeo.90.3.
Rao, C., Wang, R.C., Hu, H., Zhang, W.L., 2009. Complex internal textures in oxide mineral from the Nanping No. 31 dyke of granitic pegmatite, Fujian Province, southeastern China. Can. Mineral. 47:1195–1212. http://dx.doi.org/10.3749/canmin.47.5.
René, M., Škoda, R., 2011. Nb-Ta-Ti oxides fractionation in rare-metal granites: Krásno-Horní Slavkov ore district, Czech Republic. Mineral. Petrol. 103:37–48. http://dx.doi.org/10.1007/s00710-011-0152-z.
Rub, A.K., Stemprok, M., Rub, M.G., 1998. Tantalum mineralization in the apical part of the Cinovec (Zinnwald) granite stock. Mineral. Petrol. 63:199–222. http://dx.doi.org/10.1007/BF01164151.
Shore, M., Fowler, A.D., 1996. Oscillatory zoning in minerals: a common phenomenon. Can. Mineral. 34, 1111–1126.
Spilde, M.N., Shearer, C.K., 1992. A comparison of tantalum–niobium oxide assemblages in two mineralogically distinct rare-element granitic pegmatites, Black Hills, South Dakota. Can. Mineral. 30, 719–737.
Stepanov, A., Mavrogenes, J.A., Meffre, S., Davidson, P., 2014. The key role of mica during igneous concentration of tantalum. Contrib. Mineral. Petrol. 167:1009. http://dx.doi.org/10.1007/s00410-014-1009-3.
Sweetapple, M.T., 2000. Characteristics of Sn-Ta-Be-Li-Industrial Mineral Deposits of the Archaean Pilbara Craton, Western Australia. Australian Geological Survey Organisation 0 642 39864 X Record 2000/44.
Tindle, A.G., Breaks, F.W., 2000. Columbite-tantalite mineral chemistry from rare-element granitic pegmatites: Separation Lake area, NW Ontario. Canada. Miner. Petrol. 70: 165–198. http://dx.doi.org/10.1007/s007100070002.
Tindle, A.G., Breaks, F.W., Webb, P.C., 1998. Wodginite-group minerals from the Separation Rapids rare-element granitic pegmatite group, northwestern Ontario. Can. Mineral. 36, 637–658.
Van Lichtervelde, M., Salvi, S., Béziat, D., Linnen, R.L., 2007. Textural features and chemical evolution in tantalum oxides: magmatic versus hydrothermal origins for Ta mineralization in the Tanco lower pegmatite, Manitoba. Canada. Econ. Geol. 102:257–276. http://dx.doi.org/10.2113/gsecongeo.102.2.
Van Lichtervelde, M., Holtz, F., Hanchar, J.M., 2010. Solubility of manganotantalite, zircón and hafnon in hidghly fluxed peralkaline to peraluminous pegmatitic melts. Contrib. Mineral. Petrol. 160:17–32. http://dx.doi.org/10.1007/s00410-009-0462-x.
Wang, Y.-R., Li, J.-T., Lu, J.-L., Fan, W.-L., 1982. Geochemical mechanism of Nb,Ta-mineralization during the late stage of granite crystallization. Geochemistry 1:175–185. http://dx.doi.org/10.1007/BF03180328.
Zhu, Z.-Y., Wang, R.-C., Che, X.-D., Zhu, J.-C., Wei, X.-L., Huang, X., 2015. Magmatic-hydrothermal rare-element mineralization in the Songshugang granite (northeastern Jiangxi, China): Insights from an electron-microprobe study of Nb-Ta-Zr Minerals. Ore Geol. Rev. 65:749–760. http://dx.doi.org/10.1016/j.oregeorev.2014.07.021.